

QUANTIFYING THE IMPACT OF MOTION ON 2D GAZE ESTIMATION IN REAL-WORLD MOBILE INTERACTIONS

A PREPRINT

 **Yaxiong Lei**

University of St Andrews
St Andrews, Fife, UK, KY16 9SX
yl212@st-andrews.ac.uk

 **Yuheng Wang**


University of St Andrews
St Andrews, UK, KY16 9SX
yw99@st-andrews.ac.uk

 **Fergus Buchanan**

University of St Andrews
St Andrews, UK, KY16 9SX
fb206@st-andrews.ac.uk

 **Mingyue Zhao**

University of St Andrews
St Andrews, UK, KY16 9SX
mz201@st-andrews.ac.uk

 **Yusuke Sugano**

University of Tokyo
Tokyo, Japan
sugano@iis.u-tokyo.ac.jp

 **Shijing He**

King's College London
London, UK
shijing.he@kcl.ac.uk

 **Mohamed Khamis**

University of Glasgow
Glasgow, UK
mohamed.khamis@glasgow.ac.uk

 **Juan Ye**

University of St Andrews
St Andrews, Fife, UK, KY16 9SX
jy31@st-andrews.ac.uk

ABSTRACT

Mobile gaze tracking involves inferring a user's gaze point or direction on a mobile device's screen from facial images captured by the device's front camera. While this technology inspires an increasing number of gaze-interaction applications, achieving consistent accuracy remains challenging due to dynamic user-device spatial relationships and varied motion conditions inherent in mobile contexts. This paper provides empirical evidence on how user mobility and behaviour affect mobile gaze tracking accuracy. We conduct two user studies collecting behaviour and gaze data under various motion conditions—from lying to maze navigation—and during different interaction tasks. Quantitative analysis has revealed behavioural regularities among daily tasks and identified head distance, head pose, and device orientation as key factors affecting accuracy, with errors increasing by up to 48.91% in dynamic conditions compared to static ones. These findings highlight the need for more robust, adaptive eye-tracking systems that account for head movements and device deflection to maintain accuracy across diverse mobile context.

Keywords Mobile Eye Tracking · 2D Gaze Estimation · Calibration · Mobile Devices · User Studies

1 Introduction

Nowadays digital interfaces are an extension of our sensory input, and eye tracking on mobile devices emerges as a frontier in enhancing interactive experiences [34]. Recent advancements in mobile technologies have led to an expansion of eye-tracking applications across a diverse set of platforms, including virtual reality (VR) and augmented reality (AR) headsets, specialised eyewear, and handheld mobile devices [9, 40].

While eye-tracking technologies have reached a high level of usability in near-eye devices like VR/AR headsets [12, 42], the situation is considerably more complex for handheld mobile devices, where eye-tracking is achieved via inferring a gaze point or direction on the devices' screen mainly from their front camera. This is referred to as *appearance-based gaze estimation*, which presents the potential to enhance the accessibility of eye-tracking technologies, eliminating the need for additional hardware. At the same time, it also brings a number of challenges [31, 35, 6], as the performance of

gaze estimation model, can be significantly affected by user mobility and holding postures, and as well as environmental conditions such as lighting [53, 11].

With eye-tracking technologies, calibration is an essential step to ensure high precision of eye tracking, which is often performed at the beginning of each use [14, 52]. Once calibrated, users are required to maintain their position, especially steady head position and distance to the screen in case of calibration distortion [23, 39]. In the context of eye-tracking on handheld mobile devices, calibration does not last over an extended period, as the quality of facial images and the relative spatial relationships between the user’s head and the screen are not stable due to environmental conditions, natural head movements, and variations in holding postures and movement. For example, the distance between the face and the screen varies when users are in different motion states; e.g., 30-37 cm when sitting at a table whereas 33-42 cm when walking [24]. Previous research has studied these factors, however, there is a lack of a comprehensive understanding of how these factors interplay in real-world mobile usage scenarios.

For gaze estimation, methods can be broadly categorised based on their output: *2D* gaze estimation methods predict 2D coordinate points on the device’s screen, while *3D* gaze estimation methods predict 3D gaze vectors or directions in space [48, 56, 11]. In recent years, there has been a growing body of work using 2D gaze estimation for eye tracking on handheld devices [33, 4, 26, 53]. As an end-to-end workflow, 2D methods are easy to deploy; however, they are susceptible to changes in head pose, device orientation and camera-screen coplanarity [25, 33], and typically require a large amount of device-specific training data to tune the camera-screen plane relationship and learn the relationships between facial appearance and on-screen gaze points [5]. This reliance on device-specific data limits their applicability in some scenarios and can lead to decreased performance when users change their head pose or device orientation out of boundary of the train data [7, 35]. Given their popularity, it is essential to measure the dynamic range of changes during interaction between the user and device, and how these changes affect 2D gaze estimation accuracy in real-world use. This will be a stepping stone towards building more robust mobile eye-tracking system.

Our research is therefore driven by the overarching question: *How does motion impact the accuracy of eye tracking during natural interactions with mobile devices?* We aim to provide empirical evidence to analyse motion-related factors in such interactions, quantify their impact on gaze estimation, and identify key contributing variables. By closely examining the challenges inherent in 2D gaze estimation, we seek to highlight areas for improvement and guide future solutions. Centred around this aim, our contributions are as follows:

1. **A Novel Data Collection Framework.** We introduce a data collection framework specifically designed for mobile gaze estimation. This framework synchronizes motion and vision data (accelerometer, gyroscope, magnetometer, camera frames, and ground-truth gaze), making it possible to precisely capture both device movement and corresponding visual information. This will help reveal new insights into the effect of motion on gaze estimation.
2. **Quantitative Behavioural Modelling in Semi-Controlled Environments.** We report findings from user studies conducted under semi-controlled conditions, providing key quantitative evidence about how users naturally interact with mobile devices while performing daily tasks under varying motion states. In particular, we model typical user behaviours during mobile interactions by fusing motion sensor data and image frames, discovering distinct behavioural patterns for both within-task interaction and transitions between tasks. We observe that the head-to-screen distance remains relatively stable (0.48–2.73 cm) during a single task, while it increases significantly (7.42–10.10 cm) when switching between tasks.
3. **Empirical Evaluation of a Camera-to-Application Eye-Tracking System.** We deploy a 2D gaze estimation-based eye-tracking system in real-world application scenarios, uncovering the following challenges faced by the current approaches:
 - *Quantifying motion effects via Lasso regression:* We are the first to systematically measure the impact of various motion types on 2D gaze estimation methods using Lasso regression. Our analysis identifies head-to-screen distance, device orientation, and head movements as the most influential factors with the contributing coefficients of 35.87%, 32.29%, and 10.18% respectively.
 - *Calibration limitations in mobile usage:* Our real-world experiments demonstrate that a one-time (single) calibration at the start of interaction yields an average error of 3.43 cm on handheld devices. This highlights the importance of more frequent or adaptive calibration strategies for robust, accurate gaze tracking in mobile settings.

2 Related Work

Our research intersects four key areas: (1) gaze estimation on mobile devices, (2) eye-tracking calibration, (3) user behaviour modelling, and (4) evaluation of gaze estimation on mobile devices. This section reviews relevant projects in these areas, drawing comparisons and contrasts with our work.

2.1 Gaze Estimation on Mobile Devices

Eye tracking research on mobile devices has gained significant traction in recent years, driven by advancements in processing capabilities and camera quality [30, 11, 34, 18]. This shift aligns with the broader transition of daily tasks and communications from desktops to mobile platforms. Eye tracking technologies can be categorised into two main types: model-based approaches and appearance-based gaze estimation approaches.

The model-based gaze estimation approaches utilise the geometric contours of the user’s face and eyes to establish a spatial mapping relationship between the eyes and the gaze target. One problem of model based gaze estimation is that some of the parameters, like eye centre, are not directly observable [21, 28]. Additionally, these methods are sensitive to image quality and typically have high requirements for the usage scene [21, 38]. Mobile device usage scenarios include a variety of complex environments such as indoor-outdoor settings and static and dynamic conditions, which presents challenges for deploying model-based approaches. Consequently, only a few works have adopted them, such as EyeTab [54] and ScreenGlint [24].

The appearance-based gaze estimation approaches are an end-to-end technique that builds user facial images directly to the gaze target from learning on large-scale datasets [58, 59]. They can work under various lighting conditions and do not strictly require infrared illumination, making them more adaptable to standard mobile device cameras [58, 33]. In general, gaze estimation methods can be categorized based on their output into *2D* gaze estimation, which predicts gaze coordinates on the screen, and *3D* gaze estimation, which predicts gaze directions as 3D vectors in space [48, 11].

Methods for appearance-based gaze estimation can be further distinguished by their approach to handling head pose variability. 3D methods often involve head pose estimation and normalization techniques, where facial images are transformed into a normalized space to reduce variability due to head pose and other factors [57, 61]. By decoupling head pose from gaze direction, 3D methods can generalize better across different head poses and device configurations. However, applying 3D methods in mobile settings presents challenges, i.e. the data normalisation process is usually performed offline as its cost [43], which causes additional latency in mobile setting for real-time use. Recent approach, like EFE [7], try to reduce the pre-processing expensive cost to compute the gaze vector directly from the frame and then calculate gaze points via ray-plane intersection, leveraging the 3D gaze vector and camera parameters.

With the release of GazeCapture [33], a dataset specifically for mobile devices, and subsequent datasets such as RGBDGaze [4], 2D gaze estimation has gradually become the one of dominant algorithms behind eye tracking on mobile devices due to its simplicity and ease of deployment [34, 11]. Various variants are derived with different model input settings, from eyes [53], to various permutations of eyes, faces, landmarks, etc. [33, 22, 8, 26], and various model architectures, e.g., CNN [58, 59, 33], CNN variants combined with Recurrent Neural Networks (RNNs) [41, 29], and more recent transformers [10] to continuously achieve better results on the datasets.

These ongoing efforts continue to push the boundaries of accuracy and efficiency in mobile gaze estimation. However, the inherent challenges of mobile environments such as variable lighting conditions, diverse usage postures, and constant device movement require for robust solutions that can handle the dynamic nature of mobile interactions. Our work builds upon these foundations, focusing on the limitations of 2D gaze estimation approaches in handling head pose variability, a critical factor in real-world mobile usage scenarios.

2.2 Eye-tracking Calibration

Eye tracking systems across desktop, VR headset, glasses and mobile device platforms, need to be calibrated to achieve high precision. The calibration process is to collect the new ground truth data and use them to adjust and customise the gaze output to reflect the current spatial geometry between camera, screen and user face [34, 14]. The calibration data collection is through a user interface that guides users’ attention and requests them to fixate their gaze on specific points [13, 33, 53, 26] or follow a moving target [35, 13]. The data is fed to a calibrator to adjust the output from the original gaze estimation model. Valliappan et al.[53] applied this approach, they used support vector regression (SVR) as one-off calibrator to adjust the base 2D gaze estimation model for mobile eye tracking and achieved similar accuracy, 0.50 ± 0.03 cm, to commercial eye-tracker, the Tobii Pro 2, in the 30-second calibration data and sitting conditions.

Calibration has been extensively explored on desktop-based commercial eye-tracking instruments [34]. Sugano et al. [49] designed a incremental learning method to handle large variation of head poses. It uses mouse click as an

implicit gaze ground truth and clusters training data by head pose to create pose-specific calibrators. Huang et al. [23] applied linearity of saccade to correct gaze prediction errors and reduce the calibration distortion. Pi and Shi [46] observed that head motion causes a systematic degradation in performance due to changes in head position. Based on this finding, they propose a position-dependent linear homography-based method to correct the raw gaze estimates acquired from a remote eye tracker. Li et al. [37] explored the correlations between gaze estimation errors and facial action units via Monte Carlo. This technique based on repeated random sampling is used to predict the variability in eye tracking accuracy, particularly under challenging conditions. By simulating scenarios where accuracy might decrease, they employ Monte Carlo to anticipate gaze estimation errors, enabling timely recalibration.

These studies have primarily focused on desktop or static scenarios. However, the mobile context introduces additional complexities due to frequent changes in device orientation, head posture, and environmental conditions. Our work addresses this gap by focusing specifically on calibration for appearance-based 2D gaze estimation on handheld mobile devices. We aim to study the challenges caused by mobility and perform empirical analysis to identify the key factors and quantify their impact to the precision of 2D gaze estimation.

2.3 User Behaviour Modelling on Handheld Mobile Devices

The transition to mobile devices necessitates understanding user interaction patterns and their impact on gaze estimation. Mobile devices, equipped with sensors, offer real-time insights into user behaviour. Previous research has extensively explored aspects of user attention and behaviour in mobile contexts. Studies have investigated attention interruptions in interaction [1, 15], attention switching [47], and attention allocation in everyday life [6]. For instance, Adamczyk et al. [1] and Fogarty et al. [15] examined the effects of interruptions and the predictive value of sensor data in gauging interruptibility. Jiang et al. [27] and Steil et al. [47] demonstrated innovative uses of device cameras and head-worn cameras to track visual attention and predict bidirectional attention shifts.

In gaze estimation, recognising users behaviours is crucial, as they impact on mobility conditions and holding postures. Huang et al. [24] used front camera to record face-to-screen distances when users are in various activities. Lei et al. [35] evaluated the effect of mobility conditions on the usability of gaze interfaces, and conclude that mobility such as walking has a significant knocking effect on the gaze interfaces that requires high eye tracking accuracy such as smooth pursuit. However, user behaviour modelling in the context of eye-tracking on handheld mobile devices is under-investigated. There are only a few datasets that record gaze data and facial images, including MPIIGaze [60], EyeDiap [16] and TableGaze [25]. For example, GazeCapture [33] dataset and RGBDGaze [4] dataset records IMU data only while collecting gaze ground truth data. There are no datasets nor studies that record IMU sensor data and eye-tracking data when users are performing daily tasks on their devices.

Our paper aims to bridge the gap, encouraging users to perform various types of tasks on their phones under different motion conditions. The data will help us understand their behaviours under different tasks and as well as when switching tasks. The understanding will uncover insights on how user behaviours impact gaze estimation.

2.4 Robustness Evaluation of Gaze Estimation

Evaluating gaze estimation on mobile devices presents unique challenges due to the dynamic nature of handheld device usage. Unlike fixed desktop or head-mounted devices, mobile eye-tracking systems must contend with constantly changing spatial relationships between the user’s eyes, the device’s camera, and the screen. This variability necessitates a comprehensive understanding of the factors affecting gaze estimation accuracy in mobile contexts.

Several key variables have been identified as significant contributors to performance degradation. Image resolution is one such factor; higher resolutions improve accuracy, while lower resolutions can hinder the model’s ability to predict gaze points [61]. Lighting conditions also play a crucial role; uneven illumination, shadows, and glares compromise gaze prediction, and models trained on limited lighting conditions struggle to generalize to new environments [61, 55]. Facial occlusions further exacerbate the problem, with partially occluded faces causing significant decreases in performance [59].

Head pose and head-to-screen distance are critical factors affecting accuracy. Models experience a performance drop of up to 34.6% when encountering unseen head poses of $\pm 40^\circ$, highlighting the sensitivity to head orientation [55]. Valliappan et al. [53] demonstrated that precision decreases from 1.35 cm to 3.22 cm as the head deviates up to $\pm 25^\circ$ in roll, pan, and tilt. They also found that as the face ratio (the size of the face relative to the screen) decreases from 0.75 to 0.10—indicating increased head distance—the error increases from 0.83 cm to 2.63 cm. Similarly, increasing the face-to-screen distance from 25 cm to 40 cm results in an error increase from 1.21 cm to 1.64 cm [24].

Variable device holding patterns introduce additional challenges. Khamis et al. [31] found that front cameras capture users’ full faces only 29% of the time during unconstrained use, due to the diversity of holding postures. Mobility

further impacts performance; gaze estimation errors increase from 0.95 cm when users are sitting to 2.05 cm when walking, emphasizing the need for motion-adaptive techniques in mobile contexts [35].

While these studies provide valuable insights, many were conducted in controlled or static environments, which may not fully capture the range of movements and usage patterns associated with handheld devices in real-world settings. Our research aims to address this gap by focusing specifically on dynamic mobile scenarios, exploring how motion impacts gaze estimation accuracy during natural interactions, and utilized Lasson regression process to quantify the effects of motion in each direction.

3 Eye Tracking System

Our work aims to understand interactive impact factors between the prediction of 2D gaze estimation and body motion. To support this analysis by empirical evidence, we design and develop a data collection framework for mobile gaze estimation that simultaneously collects eye tracking and motion data. This section provides an overview of our framework design, which includes the Eye Tracking Module, Calibration Module, Evaluation Module, and Motion Sensing Module, as illustrated in Figure 1.

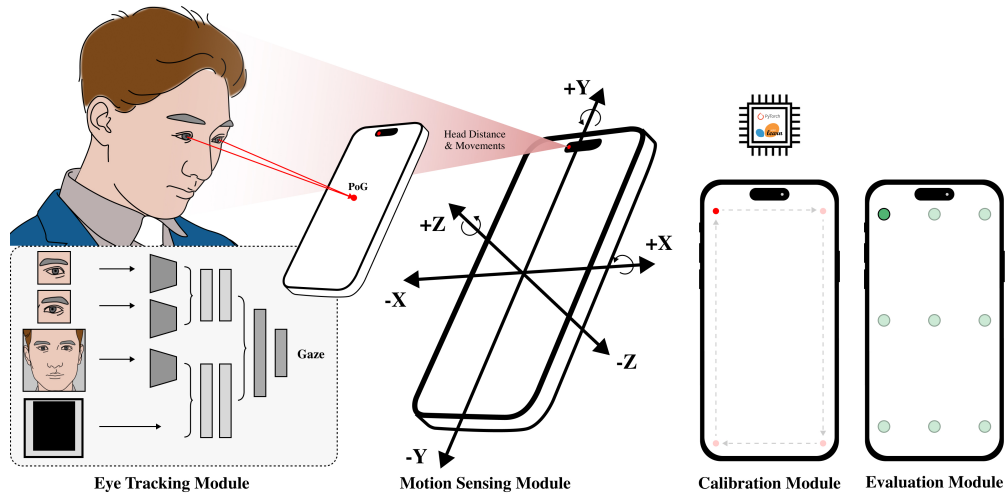


Figure 1: Overview of the experimental mobile eye tracking system.

3.1 Eye Tracking Module

The Eye Tracking Module is the core component of our framework, providing essential signals for gaze estimation. We adopted a server-client architecture, similar to established handheld mobile device eye tracking systems [35, 32]. The client-side, developed using Flutter [20], captures data, while the server-side handles model real-time inference using PyTorch and scikit-learn [44, 45]. Clients and servers communicate with each other via Wi-Fi using Transmission Control Protocol (TCP), ensuring efficient data transfer.

Our module interfaces with the device’s front-facing camera, capturing video at 30 frames per second (fps). Each frame undergoes processing to detect facial landmarks using Google’s ML Kit [19]. This step typically takes 10-25ms per frame. As our focus is to study the key impact factors in 2D appearance-based gaze estimation, especially head-to-screen distances, head movement, and device orientation, we intentionally do not rectify head positions in facial images. This decision differs from the common practice in 3D gaze estimation pipeline where head position rectification is often applied to address head movement variability [56].

The server is equipped with the PyTorch and scikit-learn frameworks [44, 45] to decouple gaze estimation models that cannot run at high speeds on mobile devices for long periods of time due to battery limitations. The model is based on the [33] architecture, pre-trained on GazeCapture [33] and fine-tuned on device-specific data from the RGBDGaze dataset [4]. The model has an average Euclidean error of 2.05 cm on the test set and can be used as a reasonable feature extractor for our 2D gaze estimation task.

3.2 Calibration Module

The Calibration Module consists of a user interface for data collection and a backend for training and storing calibration models. Users fixate their gaze on a moving dot that traverses the screen boundary, allowing the system to collect face images and corresponding gaze predictions. Based on pilot testing and previous research [32, 35], we implement a 5-second data collection cycle, balancing accuracy and user comfort, typically gathering between 125 and 150 data pairs.

The collected data is processed through the gaze estimation model, extracting high-dimensional visual feature maps from the first fully connected layer. These feature maps are synchronised with the ground truth gaze points to train a Support Vector Regression (SVR) model to perform inference instead of the remaining fully connected layers. We chose SVR for its effectiveness as a lightweight calibration method [35, 33, 53], supported by comparative studies [2].

3.3 Evaluation Module

The Evaluation Module consists of a user interface for data collection and a back-end for data storage and analysis. The evaluation interface displays dots on the screen in a random order, with potential locations illustrated in Figure 1. The interface allows for varying the sequence of dot appearances and the number of dots (ranging from 3 to 9) as well as different locations. In this study, we use a setup of 9 points appearing in a random order to evaluate accuracy across different screen areas.

3.4 Motion Sensing Module

The Motion Sensing Module captures the device’s real-time motion and tracks changes in the user’s head and body movements. This module utilises the built-in IMU and the front camera. By employing the Flutter framework’s `sensor_plus` package and Google’s ML Kit, the module accesses and records a rich set of sensor data, including raw and processed acceleration, device rotation, ambient magnetic fields, and head-related movements, as detailed in Table 1.

Device Movement: The module records device manipulation by tracking changes in orientation and movement using IMU data. This helps understand how device handling affects gaze estimation accuracy.

Head Movement: The Motion Sensing Module captures head movement using the front camera, including the head’s distance from the device and its orientation (pose). Head pose is computed from facial landmarks detected by ML Kit, represented in terms of Euler angles (pitch and yaw).

Since no out-of-the-box API measures head distance, we developed a custom method based on the linear proportional relationship between interpupillary distance and the distance from the eyes to the phone screen. We manually measured the physical interpupillary distance (IOD_{Physical}) and the distance from the interpupillary centre to the camera ($D_{\text{Head-Camera}}$) using a ruler. The interpupillary distance within the image frame (IOD_{Frame}) is then calculated based on facial landmarks detected in the images. These measurements are used to establish a regression model, as shown in Eq. 1, to learn the coefficients β_0, β_1 , and the random error ϵ , allowing us to approximate $D_{\text{Head-Camera}}$. This method is implemented in the motion sensing module to provide real-time estimations of head-to-camera distance, as depicted in Figure 2.

$$D_{\text{Head-Camera}} = \beta_0 + \beta_1 \times \frac{IOD_{\text{Physical}}}{IOD_{\text{Frame}}} + \epsilon \quad (1)$$

Sensor Events	Frequency	Dimension	Description
UserAccelerometer	50Hz	X,Y,Z	Acceleration (m/s^2) without the effects of gravity.
Accelerometer	50Hz	X,Y,Z	Acceleration (m/s^2) with the effects of gravity.
Gyroscope	50Hz	X,Y,Z	Device rotation.
Magnetometer	50Hz	X,Y,Z	Ambient magnetic field surrounding the device.
Head distance	30Hz	distance	Distance between the eye center and the device camera.
Head pose	30Hz	Pitch, Yaw	Head orientation relative to the camera.

Table 1: Description of sensor data collected and estimated by the Motion Sensing Module.

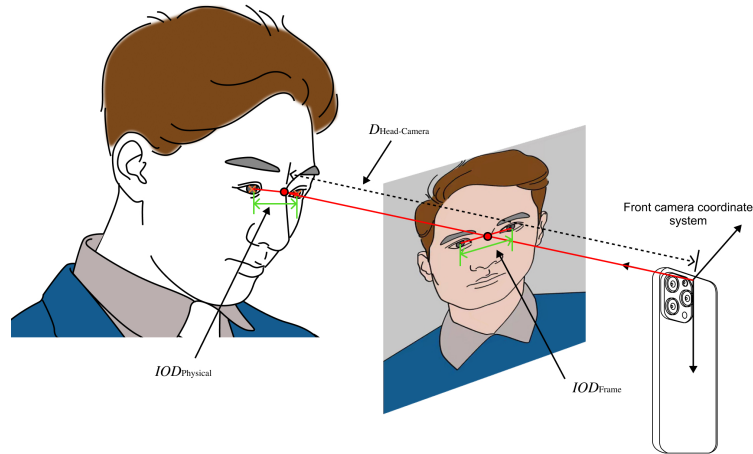


Figure 2: Head-to-camera distance calculation.

4 Study Design

To systematically investigate the impact of motion patterns and behaviours during daily interaction between user and mobile device on gaze estimation accuracy, we divided our primary research question - *How does motion impact the precision of gaze estimation during natural interactions with mobile devices?* - into three sub-questions:

- Q1 - **Motion Pattern Exploration:** What distinct motion patterns emerge when users interact with mobile phones, and is there discernible regularity in these patterns?
- Q2 - **Motion Impact on Performance:** To what extent do various motion conditions and postural changes affect the accuracy of 2D gaze estimation?
- Q3 - **Factor identification:** Which specific dynamic variables significantly contribute to performance degradation in 2D gaze estimation?

To address these questions, we designed the user studies depicted in Figure 3. The User Study 1 focuses on understanding motion patterns and behaviours during typical user interaction tasks, while the User Study 2 links these motions to gaze estimation accuracy, providing a foundation for subsequent analysis.

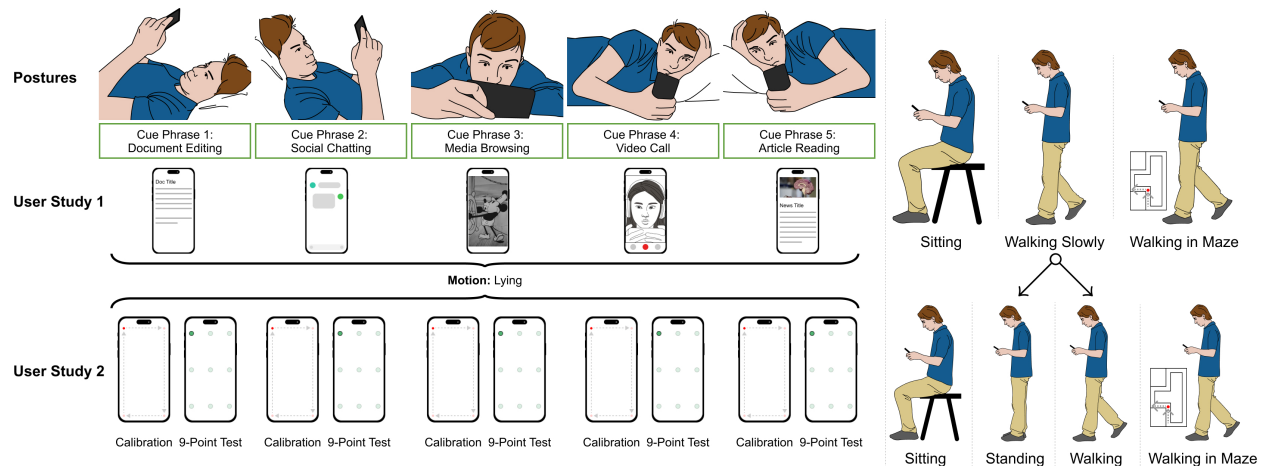


Figure 3: Schematic overview of the user study design. User Study 1 explores spatial dynamics of mobile interactions across various daily tasks and motion conditions. User Study 2 evaluates 2D gaze estimation performance under simulated real-world scenarios.

4.1 User Study 1 – Interaction Pattern

The objective of user study 1 is to analyse the spatial relationships and motion behaviours exhibited by users while interacting with their mobile devices during everyday tasks. This involves observing and recording a variety of motion states such as lying, sitting, standing, walking slowly, and navigating through a maze, to simulate real-world scenarios. These conditions are chosen based on an extensive literature review [24, 4, 58, 25, 16, 35, 50] and are further supplemented by our maze navigation condition to simulate complex user movements encountered in daily life.

To ensure ecological validity, we selected tasks that mimic daily usage patterns on handheld devices. Specifically, we asked participants to perform a series of routine tasks under each condition including, *document editing* simulates note-taking or drafting emails, *social chatting* represents quick message replies via popular apps like WhatsApp, *social media browsing* (e.g., Instagram, Twitter) captures casual content consumption, *video calling* allows for real-time communication or short call simulations, and *news reading* aligns with web-based article consumption, with cue phrases provided to guide task execution as shown in Table 2. These tasks were chosen for their prevalence in everyday life and for covering a spectrum of interactions (e.g., heavy typing, continuous scrolling, periodic glances).

To further reduce bias, tasks were *randomized in order* for each participant. Participants received a short 1–2 minute training/familiarization session with the experiment application before starting. This ensured that they understood how to hold and interact with the device under different motion conditions. We also encouraged them to use their natural usage posture (e.g., one-handed vs. two-handed) to maximize authenticity of the recorded behavioural data.

Task	Cue Phrase
Document editing	“Create a new document using your preferred document editing app and write today’s diary entry.”
Social chatting	“Open your preferred social media app, such as WhatsApp, and respond to any unread messages.”
Social media browsing	“Open a social media app like Instagram to browse content or like posts.”
Video calling	“Use your preferred video calling app to either simulate a video call or engage in a brief call with a friend.”
News reading	“Open your preferred news app to read some articles.”

Table 2: Cue Phrases for switching tasks

Data collection utilises motion sensing module of our application, which captures a rich dataset of motion sensor readings (accelerometer, gyroscope, and magnetometer) and camera-based measurements (head pose and distance), as detailed in Table 1.

4.2 User Study 2 – Impact and Factors

User Study 2 aims to assess the performance of a 2D gaze estimation method under simulated real-world conditions by correlating the frequency and intensity of motion patterns with model prediction errors. This study extends the first by examining how well the current mobile eye-tracking systems perform under typical everyday tasks (see Table 2). We replicate cue-guided tasks from user study 1 to evoke similar postures and behaviours under controlled motion conditions, including lying, sitting, standing, walking, and walking in maze. Each participant produces 25 pairs of calibration and test data, corresponding to 5 motion conditions and 5 cue-guided tasks. For each cue-guided task of a motion condition, participants were subjected to a calibration and 9-point test procedure. This collected dataset enables a systematic evaluation of how factors such as head-to-screen distance, head movements, and device orientation affect gaze estimation accuracy in dynamic, mobile contexts.

4.3 Comparison of User Study 1 and User Study 2

While User Study 1 focuses on observing and analysing users’ natural interaction patterns with their mobile devices under various motion conditions and tasks, User Study 2 specifically evaluates how these motion patterns impact the performance of a 2D gaze estimation system. In User Study 1, participants interact with their devices naturally, and we collect motion and spatial data to understand typical behaviours and patterns, without introducing any gaze estimation tasks that might alter their natural interaction. In contrast, User Study 2 involves participants performing similar tasks but includes gaze estimation procedures, such as calibration and testing, to measure the accuracy of gaze prediction under different motion conditions. The inclusion of calibration and testing in User Study 2 means that participants may

adjust their interaction patterns slightly due to the demands of the gaze estimation tasks. However, by replicating the tasks and conditions from User Study 1, we aim to maintain consistency in the behaviours elicited.

This dual-study design allows us to first characterize the motion patterns in natural usage (addressing Q1) and then directly assess their impact on gaze estimation performance (addressing Q2 and Q3). By comparing the findings from both studies, we can identify which aspects of user motion and behaviour are most critical for gaze estimation accuracy and develop strategies to mitigate their negative effects.

5 User Study and Data Collection

This section delineates the methodological approach employed in our user studies and data collection processes. The research protocol was approved by the university ethics committee (reference number CS16900), ensuring adherence to ethical standards in human subject research.

5.1 Participants

A cohort of 10 participants (4 females, 6 males) was recruited from the undergraduate and postgraduate communities at our university. The sample's age distribution ranged from 21 to 31 years ($M = 26.4$, $SD = 3.14$). All participants possessed either normal or corrected-to-normal vision. Among the participants, 50% ($n = 5$) wore corrective lenses, with mean myopia measurements of 299 diopters ($SD = 96.45$) for the left eye and 334 diopters ($SD = 148.40$) for the right eye.

Given the study's focus on spatial and motion impacts, we collected additional anthropometric data. Participants' heights ranged from 155 cm to 185 cm ($M = 172.5$ cm, $SD = 10.55$). The arm length of the dominant hand varied from 52 cm to 63 cm ($M = 57.2$ cm, $SD = 3.96$), while interpupillary distances ranged from 6.02 cm to 6.50 cm ($M = 6.32$ cm, $SD = 0.23$). A demographic questionnaire assessed participants' technology familiarity and usage patterns. On a 5-point Likert scale (1 = least familiar, 5 = most familiar), participants reported high familiarity with mobile phone usage ($M = 4.5$, $SD = 0.81$) but low familiarity with gaze technologies ($M = 1.5$, $SD = 0.5$). The frequency of mobile phone use while walking was moderate ($M = 2.9$, $SD = 1.04$, on a scale where 1 = lowest frequency and 5 = highest frequency).

5.2 Apparatus and Environmental Setting

The experimental setup comprised a client-server architecture. The client device was an Apple iPhone 13 Pro Max (6.7-inch display, 240 grams, 256 GB storage, iOS 16). This was paired with a high-performance server (Intel i9-13900HX processor, NVIDIA RTX 4080 GPU, 32GB RAM) for real-time data processing and storage. The system achieved a gaze inference frequency of 25-30 fps.

The user studies take place in a large lecture room measuring 8 m in width and 20 m in length. A rectangular area of 5 m \times 10 m is transformed into a concave-shaped maze and the walk path enclosed by soft cushions. Chairs and loungers are arranged in a 3 m \times 3 m area and placed in a corner on the same side as the maze. The rest of the room is left empty. The lighting in the room is primarily natural light, supplemented by artificial illumination.

5.3 Experiment Procedure of User Study 1: Understanding User-Device Interaction Patterns

We briefed the purpose, apparatus and procedures of the user studies to all the participants before the start of experiments. To ensure a natural interaction and mitigate privacy concerns, participants were instructed to use their personal phones for the tasks prompted by cue phrases. Simultaneously, our experimental phone was affixed to the rear of their device to capture relevant data, including IMU and facial images from the camera. However, we recognise a potential drawback of this approach: the combined weight of the two phones might alter participants' handling and mobility of their devices.

The experiment is designed with 5 types of tasks and all of these are guided to be executed by cue phrase as shown in Table 2. We do not have specific requirements for task execution but provide corresponding suggestions. For instance, we recommend using an Instagram-like app for the social media browsing task, and Microsoft Office or Google Docs for the document editing task. In the task of chatting and dialogues, headphones could be worn to protect privacy.

The procedure of the experiment is shown in Figure 3. Participants are firstly guided to the lying condition where they can lie on a big soft sofa in the experiment room. Once the participant is lying down, the system begins to record data. Then the participant will be guided through a series of tasks on their mobile phone using short cue phrases. Each task lasts between 4 and 6 minutes, and each condition comprising these 5 tasks takes approximately 15 to 20 minutes. The duration of the user study on each participant is between 60 and 90 minutes.

With 40 trials of 10 participants and 4 motion conditions, after data cleaning, we have collected 1,232,633 events for each of accelerometer, gyroscope and magnetometer and 739,578 samples for head movement and angle events extracted from image frames.

Sensor \ Motion	Lying	Sitting	Walking Slowly	Walking in Maze	Total
IMU	311,438	310,802	324,690	285,703	1,232,633
Camera	186,862	186,481	194,814	171,421	739,578

Table 3: Distribution of data samples across motion conditions and sensor types in User Study 1

5.4 Experiment Procedure of User Study 2: Impact and Factor Analysis

User Study 2 aims to assess the impact of mobility on 2D gaze estimation accuracy in simulation of a real-world usage scenario. Participants are instructed to use our experimental device directly, which is equipped with custom-developed gaze calibration and test tasks. The protocol requires participants to naturally alter their device holding postures for each task under different motion conditions while performing both calibration and test tasks.

We collected 803,241 time-stamped events across 50 trials involving 10 participants under 5 motion conditions. Table 4 presents the number of samples from both IMU and camera sensors under each motion condition and experimental phase. More specifically, we collected 137,011 IMU and 82,205 camera events during calibration, and 666,230 IMU and 399,736 camera events during the 9-point gaze tests.

Samples \ Motion	Lying	Sitting	Standing	Walking	Walking in Maze	Total
Calibration IMU	27,471	27,230	27,949	27,652	26,709	137,011
Calibration Camera	16,482	16,338	16,769	16,591	16,025	82,205
9-Point Test IMU	130,419	133,647	135,409	133,512	133,243	666,230
9-Point Test Camera	78,251	80,188	81,245	80,107	79,945	399,736

Table 4: Distribution of data samples across motion conditions, sensor types, and experimental phases in User Study 2

5.5 Data Preprocessing and Feature Extraction

In the following, we illustrate the pre-processing and feature extraction steps on IMU data.

5.5.1 Preprocessing

During preprocessing, IMU sensor events are synchronised with camera frames according to their timestamps. Special care is taken to synchronise their heterogeneous sampling frequencies. Specifically, we use neighbour interpolation [36] to estimate the IMU sensor values at the exact moments when camera frames are captured. This method allows us to accurately pair each camera frame with the corresponding IMU data, providing a synchronised dataset for further analysis.

We perform two denoising steps. We apply a Butterworth low-pass filter to smooth the IMU sensor data [3], and filter out unrealistic head distances based on human ergonomic thresholds. That is, the samples of head distance distribution can be modelled as an approximate Gaussian. Lower one-sided confidence interval with 95% probability suggests that the head distance threshold is around 100 cm. If the value is larger then 100 cm, it means the participant does not look at the screen.

5.6 IMU Feature Extraction

Feature extraction is crucial in analysing complex, high-dimensional time-series data from IMUs. We adopt a classic feature engineering method from human activity recognition [3], focusing on three categories of features: *Frequency Domain*, *Time Domain*, and *Cross-channel* features.

Frequency Domain Features play a critical role in identifying the periodic characteristics and predominant frequencies of sensor signals. These features are derived through the transformation of time-domain data into the frequency spectrum using Fast Fourier Transform (FFT). Significant frequency domain features include mean (calculated as $\frac{1}{N} \sum_{i=1}^N x_i$,

where x_i represents the amplitude of the i^{th} frequency component, and N is the number of frequency components), variance, standard deviation, skewness, kurtosis, direct component (DC), and the top 4 amplitudes along with their corresponding frequencies. Such features are particularly effective in recognising cyclical activities like walking or running.

Time Domain Features, extracted directly from the sensor data over a time window, provide fundamental statistical insights. The features include mean (given by $\frac{1}{N} \sum_{i=1}^N x_i$, where x_i is the i^{th} time-domain sample and N is the total number of samples in a window), variance, standard deviation, mode, min/max, range, and zero-crossing rate. These features capture the basic motion attributes including range, intensity, and variability, which are vital for detecting general motion patterns and activity intensity.

Cross-channel Features examine the interrelationships between different sensor axes or channels. Considering that smartphone sensors like IMUs typically offer three-dimensional data (X, Y, Z axes), it is crucial to analyse the correlations and interactions among these channels. Features in this category include cross-correlation coefficients, represented by $CC_{xy}(k) = \frac{\sum_i (a_{x,i} - \bar{a}_x)(a_{y,i+k} - \bar{a}_y)}{\sqrt{\sum_i (a_{x,i} - \bar{a}_x)^2 \sum_i (a_{y,i+k} - \bar{a}_y)^2}}$, where $a_{x,i}$ and $a_{y,i+k}$ represents x- and y-axis sensor data at i th and $i+k$ th (the lag) timestamps, and \bar{a}_x and \bar{a}_y represents the mean x- and y-axis sensor data. This cross-correlation coefficients quantify the degree of similarity and the lead-lag relationship between the time-series data of different axes. Cosine similarity $\frac{\vec{a}_i \cdot \vec{a}_j}{\|\vec{a}_i\| \|\vec{a}_j\|}$ assesses the directional alignment between two multi-axial data vectors \vec{a}_i and \vec{a}_j at the i th and j th timestamps, providing insight into their relative orientation. The synthetic mean is a composite metric encapsulating the overall magnitude of motion by combining the squared sum of multi-axial signals: $a_i = \sqrt{(a_{x,i})^2 + (a_{y,i})^2 + (a_{z,i})^2}$. These features are instrumental in understanding complex movements, such as the coordination in limb movements during running or multi-axial activities like climbing stairs.

6 Data Analysis and Results

6.1 User Study 1 – Interaction Pattern

To understand various motion patterns and behaviours during daily interaction between user and device, we perform analysis from raw motion data to user behaviour patterns.

- *Motion Data Visualisation* to examine their value range and interacting relationships among various motion conditions;
- *Mobility Patterns* to investigate regularity across motion conditions and behaviours of interaction.

6.1.1 Motion Data Visualisation

Figure 4 presents the box plots of raw motion data under each motion condition, and Figure 5 visualises the distribution of extracted features under each motion condition. We illustrate the analysis on each dimension in the following.

Head distance: Head distance states the distance between the eyes and the camera, approximately indicating the distance between the eyes and the screen. The values in Figure 4 show the mean and variation of distance in different motion conditions when the participant interacts with the device. Throughout user study 1, the largest variation in distance resides in lying ($M = 31.37\text{cm}$, $SD = 10.09\text{cm}$), followed by sitting ($M = 34.61\text{cm}$, $SD = 8.44\text{cm}$) and two dynamic conditions: walking slowly ($M = 31.07\text{cm}$, $SD = 7.01\text{cm}$), and walking in maze ($M = 33.13\text{cm}$, $SD = 7.57\text{cm}$). The greater variability in lying and sitting may be due to the fact that sofas and chairs can support the body and there is more room for movement of the arms and hands; therefore, postural changes are more flexible.

Head Euler Angles (Pitch, Yaw): The pitch and yaw angles are key indicators of head orientation. All participants are accustomed to placing the device below head level, so the mean of pitch angles is positive and the mean of yaw angle is close to 0; more specifically, lying ($M_{pitch} = 1.23$, $SD_{pitch} = 9.61$, $M_{yaw} = -1.24$, $SD_{yaw} = 10.96$), sitting ($M_{pitch} = 2.15$, $SD_{pitch} = 8.09$, $M_{yaw} = -0.73$, $SD_{yaw} = 7.49$), walking slowly ($M_{pitch} = 1.25$, $SD_{pitch} = 7.68$, $M_{yaw} = -0.57$, $SD_{yaw} = 5.20$), and walking in maze ($M_{pitch} = 2.19$, $SD_{pitch} = 10.72$, $M_{yaw} = 0.35$, $SD_{yaw} = 7.34$). Similar to the head distance, the variation of the Euler Angle of the head under static conditions is larger than that under dynamic conditions. However, the changes of posture during walking in the maze are similar to those of sitting. That is, when users are finding and avoiding obstacles in the maze, they tend to move their phones out of their viewing range.

User Accelerometer (X, Y, Z): As users are required to interact with the device by various tasks, they are less likely to perform high-intensity activities; therefore, their accelerometer readings remain stable: lying ($M_X = 0.00$,

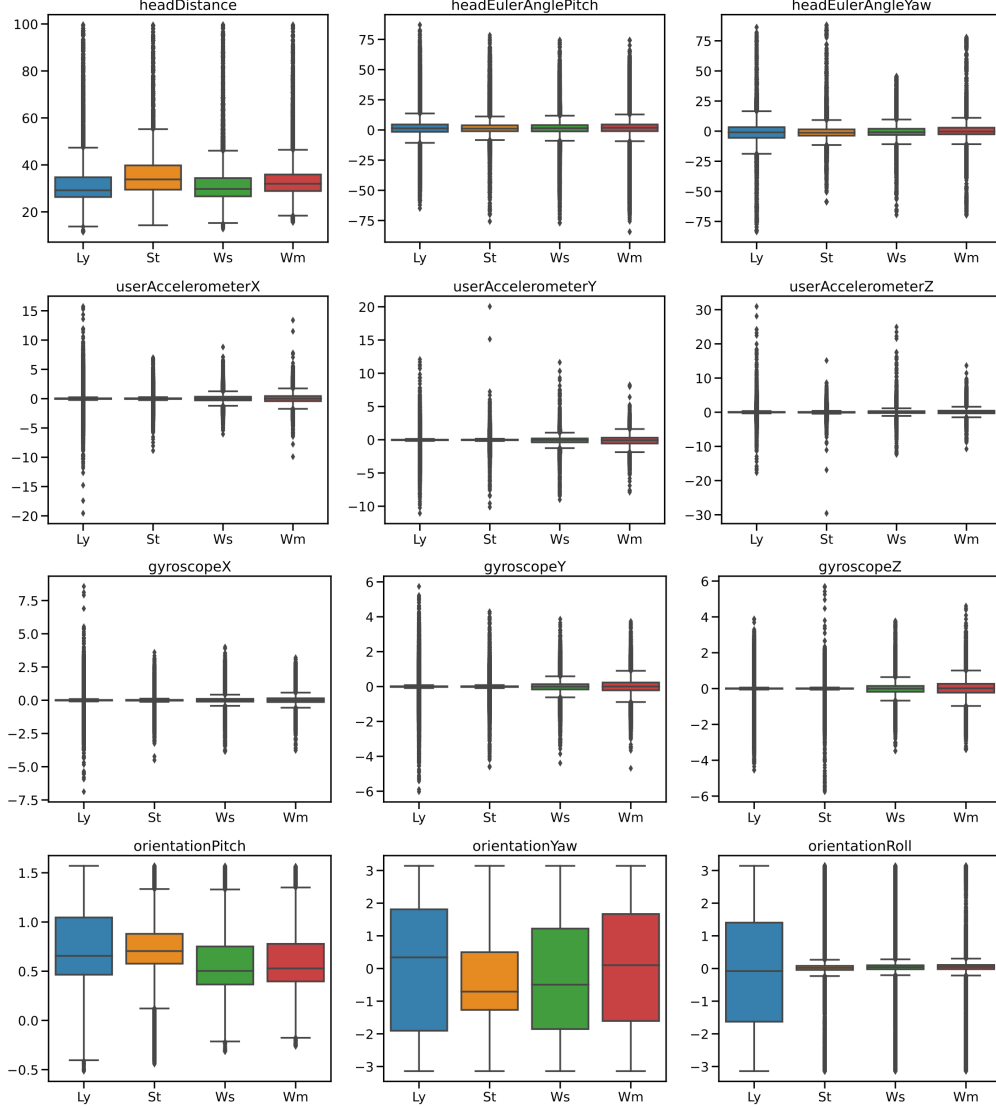


Figure 4: Box plots of sensor data under each motion condition: *Ly* for lying, *St* for sitting, *Ws* for walking slowly and *Wm* for walking in maze.

$SD_X = 0.49$, $M_Y = -0.05$, $SD_Y = 0.38$, $M_Z = 0.01$, $SD_Z = 0.56$), sitting ($M_X = 0.01$, $SD_X = 0.32$, $M_Y = -0.03$, $SD_Y = 0.26$, $M_Z = -0.01$, $SD_Z = 0.40$), walking slowly ($M_X = 0.02$, $SD_X = 0.59$, $M_Y = -0.10$, $SD_Y = 0.55$, $M_Z = 0.04$, $SD_Z = 0.61$), and walking in maze ($M_X = 0.01$, $SD_X = 0.72$, $M_Y = -0.14$, $SD_Y = 0.67$, $M_Z = 0.07$, $SD_Z = 0.77$). The variation in user accelerometer caused by changing posture or task between sitting and lying is smaller than that under dynamic conditions. When users are sitting and lying down, the change in posture is caused by the deflection of the head and arms, which is less than the acceleration generated by the moving actions.

Gyroscope (X, Y, Z): The gyroscope can obtain data on how fast the orientation of the device changes, and the greater the absolute value of the reading, the faster the angle changes. The mean value of the gyroscope is close to 0 in the three axes for all the motion conditions. The variation is much greater and the change caused by the two walking conditions is greater than that of sitting and lying down; that is, lying ($M_X = 0.00$, $SD_X = 0.25$, $M_Y = 0.00$, $SD_Y = 0.26$, $M_Z = 0.00$, $SD_Z = 0.21$), sitting ($M_X = 0.00$, $SD_X = 0.18$, $M_Y = 0.00$, $SD_Y = 0.18$, $M_Z = 0.00$, $SD_Z = 0.17$), walking slowly ($M_X = 0.00$, $SD_X = 0.23$, $M_Y = -0.01$, $SD_Y = 0.33$, $M_Z = -0.01$, $SD_Z = 0.39$), and walking in maze ($M_X = 0.00$, $SD_X = 0.28$, $M_Y = 0.01$, $SD_Y = 0.40$, $M_Z = 0.02$, $SD_Z = 0.49$).

Orientation (Pitch, Yaw, Roll): The pitch, yaw and roll angles are key indicators which are similar with the head pose to show device orientation. The variation of pitch is similar to that of yaw, and lying has the largest variation, followed by the two walking conditions; more specifically, lying ($M_{Pitch} = 0.74$, $SD_{Pitch} = 0.39$, $M_{Yaw} = 0.02$, $SD_{Yaw} = 1.97$), sitting ($M_{Pitch} = 0.73$, $SD_{Pitch} = 0.29$, $M_{Yaw} = -0.28$, $SD_{Yaw} = 1.47$), walking slowly ($M_{Pitch} = 0.58$, $SD_{Pitch} = 0.30$, $M_{Yaw} = -0.29$, $SD_{Yaw} = 1.80$), and walking in maze ($M_{Pitch} = 0.59$, $SD_{Pitch} = 0.29$, $M_{Yaw} = 0.03$, $SD_{Yaw} = 1.87$). Lying has resulted in a big difference in the mean of Roll and a larger variation than the other conditions; that is, lying ($M_{Roll} = -0.15$, $SD_{Roll} = 1.68$), sitting ($M_{Roll} = 0.04$, $SD_{Roll} = 0.51$), walking slowly ($M_{Roll} = 0.05$, $SD_{Roll} = 0.28$), and walking in maze ($M_{Roll} = 0.03$, $SD_{Roll} = 0.28$). In addition, lying exhibits the greatest variation in head distance and orientation. The two walking conditions exhibit a greater variation than static conditions on accelerometer and gyroscope readings.

Relationships of Motion Conditions We present t-SNE (t-Distributed Stochastic Neighbour Embedding) plots of extracted sensor features from all the participants under these motion conditions in Figure 5. The t-SNE is usually applied for data visualisation that reduces the dimensionality of high-dimensional data while preserving the relationships and structures within the data as much as possible. Overall, the t-SNE plots show a distinct separation between lying (purple) and sitting (green) conditions, while walking slowly (blue) and walking in maze (yellow) are overlapping due to their similar motion signatures. Specifically, the features under lying are most spread, followed by sitting, walking slowly and walking in maze. The spreadness suggests the variety of postures and movement. This finding is consistent with the above raw sensor data analysis.

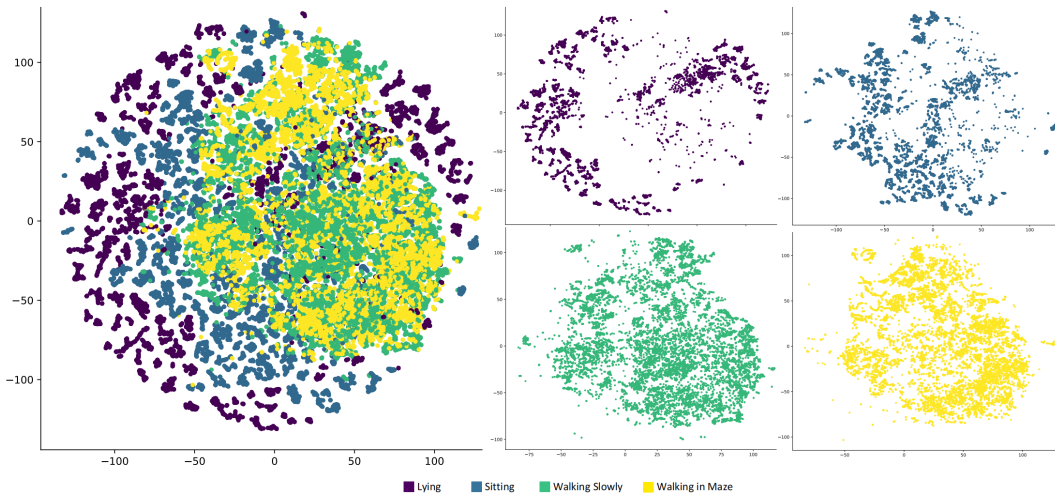


Figure 5: t-SNE plots of sensor features under each motion condition

6.1.2 Mobility Patterns

Our next task is to investigate into regularity of motion patterns; i.e., how many different patterns each participant exhibited under different motion conditions. Towards this end, we run GMM (Gaussian Mixture Models) on each participant’s data and present the box plots of the number of clusters under each motion conditions in Figure 6. Most of the participants exhibit ~ 4 clusters for lying and sitting and ~ 2 clusters for walking conditions. This suggests that there is high regularity in users’ motion patterns. The motion patterns under dynamic conditions exhibit greater stability, implying that users actively stabilise themselves while attempting to read on the screen.

Figure 7 and Figure 8 maps GMM clusters of Participant 1 on their time-series sensor data. The GMM effectively clusters data in static conditions, identifying distinct motion patterns during tasks and transitions indicated by cue phrases. On the other hand, it is difficult for GMM to recognise the transitions of tasks under dynamic conditions. All the movements are clustered to a single group. In the following, we will investigate the in-task and switch-task scenarios further.

In vs. Switch Task Using task execution and task switching as clues, we delve deeper into the data in section 6.1.1. Often users interact with phones in a dynamic and context-dependent manner. We aim to understand how users’ gaze and interaction with their devices change as they shift from active engagement in a task (in-task) to transitioning between tasks (switch-task).

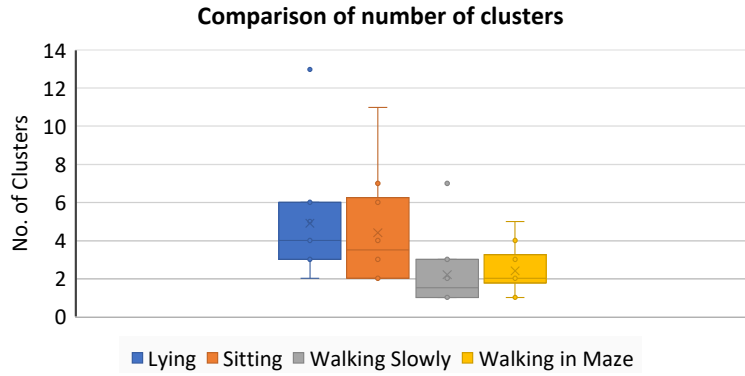


Figure 6: Comparison of the number of motion clusters under different motion conditions

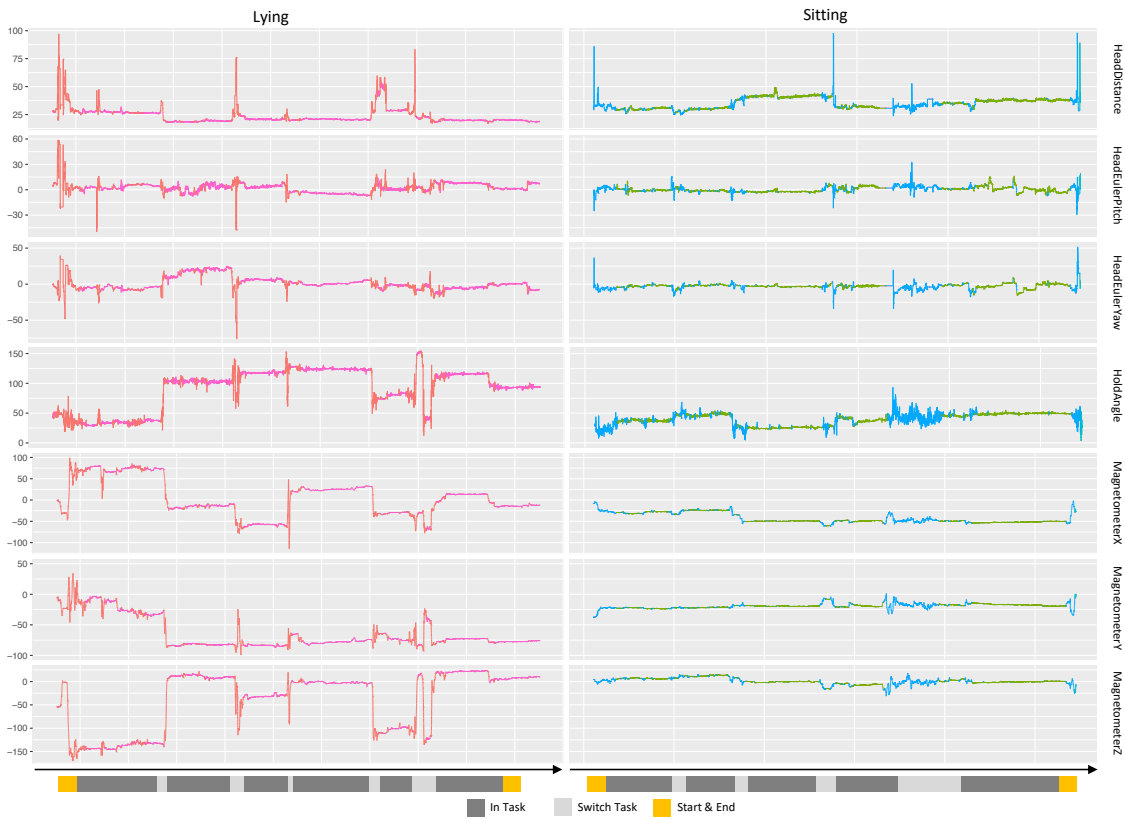


Figure 7: GMM clustering mapped to time-series sensor data on Participant 1 under static conditions

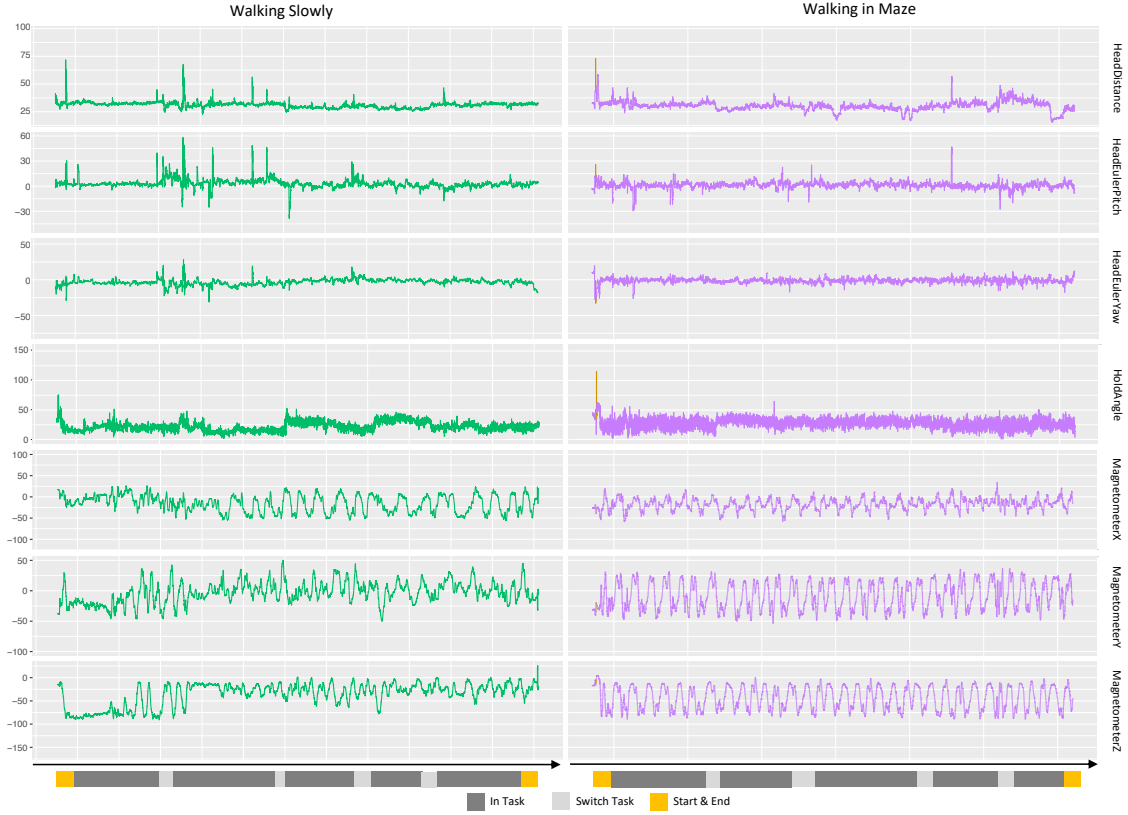


Figure 8: GMM clustering mapped to time-series sensor data on Participant 1 under dynamic conditions

Attribute \ Setting	Lying				Sitting			
	In Task		Switch Task		In Task		Switch Task	
	Mean	Std	Mean	Std	Mean	Std	Mean	Std
headDistance	23.65	2.23	31.54	10.10	41.25	0.48	34.60	8.40
headEulerAnglePitch	3.96	1.55	1.22	9.07	4.57	2.31	2.19	7.62
headEulerAngleYaw	0.60	1.80	-1.35	10.48	-3.42	2.53	-0.79	6.90
useraccelerometerX	0.00	0.08	0.01	0.49	0.00	0.19	0.01	0.31
useraccelerometerY	0.00	0.05	-0.05	0.38	0.05	0.08	-0.03	0.26
useraccelerometerZ	-0.01	0.11	0.01	0.56	-0.05	0.24	-0.01	0.40
gyroscopeX	0.00	0.04	0.00	0.25	0.10	0.09	0.00	0.19
gyroscopeY	0.00	0.04	0.00	0.26	0.00	0.19	0.00	0.18
gyroscopeZ	0.00	0.03	0.00	0.22	-0.10	0.09	0.00	0.16
orientationRoll	-0.24	0.11	-0.15	1.70	0.00	0.13	0.04	1.51
orientationPitch	0.29	0.04	0.01	1.99	1.06	1.21	-0.28	1.47
orientationYaw	0.32	0.04	0.75	0.39	0.53	0.41	0.74	1.59
HoldAngle	23.29	4.73	84.75	36.85	30.89	5.69	44.03	17.50
Velocity	0.03	0.02	0.10	0.21	0.08	0.14	0.09	0.13

Table 5: Comparison of mean and std of motion data for in task and switching task under static conditions

Tables 5 and 6 present a detailed comparison of mean and standard deviation of raw motion data in in- and switch-tasks under static and dynamic conditions. The head distance and orientation sensors such as gyroscope and accelerometer exhibit small variation in the in-task state, suggesting users maintain a relatively stable distance from their device while engaging in a task, regardless of their motion state.

Attribute	Walking Slowly		Walking in Maze							
			In Task		Switch Task		In Task		Switch Task	
	Mean	Std	Mean	Std	Mean	Std	Mean	Std	Mean	Std
headDistance	27.94	2.58	31.67	7.42	31.37	2.73	33.12	7.54		
headEulerAnglePitch	0.23	2.86	1.45	8.28	2.24	3.78	2.22	10.14		
headEulerAngleYaw	-1.84	2.82	-0.33	5.51	0.97	3.96	0.30	6.34		
useraccelerometerX	0.02	0.51	0.02	0.60	-0.02	0.60	0.01	0.72		
useraccelerometerY	-0.09	0.52	-0.11	0.55	0.01	0.57	-0.14	0.67		
useraccelerometerZ	0.03	0.52	0.05	0.62	-0.04	0.48	0.08	0.74		
gyroscopeX	0.00	0.20	0.00	0.25	0.01	0.26	0.00	0.28		
gyroscopeY	-0.03	0.34	-0.02	0.33	0.01	0.38	0.01	0.40		
gyroscopeZ	-0.04	0.42	-0.01	0.39	-0.10	0.45	0.02	0.47		
orientationRoll	-0.02	0.07	0.06	0.30	-0.02	0.22	0.03	0.48		
orientationPitch	-0.36	1.79	-0.27	1.80	-0.70	1.91	0.03	3.88		
orientationYaw	0.46	0.18	0.61	0.31	0.68	0.51	0.60	0.99		
HoldAngle	26.37	10.34	35.22	18.43	39.04	9.62	34.62	17.07		
Velocity	0.22	0.13	0.23	0.17	0.08	0.15	0.29	0.18		

Table 6: Comparison of mean and std of motion data for in task and switching task under dynamic conditions

Intuitively, switching-task reveals significant variability, with increased standard deviations across all motion data; e.g., lying: $31.54 \pm 10.10\text{cm}$, sitting: $34.60 \pm 8.40\text{cm}$, walking slowly: $31.67 \pm 7.42\text{cm}$, and walking in a maze: $33.12 \pm 7.54\text{cm}$. This indicates greater variability and potentially more head movement or changes in posture. This might reflect the users' momentary distraction or reorientation as they switch tasks, which is more pronounced when they are stationary (lying or sitting).

By further examining Table 5 and 6, we can conduct empirical analysis of user postures under different motion conditions. For example, the distance from the head to the screen under lying is the shortest; i.e., 23.65 cm, and the head is lifted upward by 3.96 degrees and deflected to the right by 0.6 degrees with respect to the device screen (Pitch = 3.96, Yaw = 0.60). When users are lying down, their phone maintains a head distance of 23.65 cm and is tilting towards the left side of the head (Pitch = 3.96, Yaw = 0.60) with holding angle of 23.29 degrees.

6.2 User Study 2 – Impact and Factors

Building upon the insights from User Study 1, this section investigates the impact of motion patterns and behaviours under various motion conditions on the performance of 2D gaze estimation and identifies the key factors contributing to the impact. As outlined in Section 4.2, User Study 2 data comprises 5 calibration data and five 9-point testing data for each motion condition, including ground truth points, facial images, and IMU sensor readings, as shown in Table 4.

In the following, we analyse the impact of motion patterns and behaviours on 2D gaze estimation:

1. *Motion Data Visualisation* to examine the distribution of each motion variables and relationships between calibrations and tests;
2. *Performance Degradation* to assess to what degree mobility decrease the performance of gaze estimation model and calibrator;
3. *Impact Factor Identification* to discover what mobility features contribute most to the degradation.

6.2.1 Motion Data Visualisation

To maintain consistency with User Study 1, we visualise the motion data from User Study 2 using box plots in Figure 9. Additionally, we compare the distributions of motion data in calibration and test procedures in Figure 13, which informs our discussion on calibration performance. We analyse each dimension as follows:

Head distance: The trends in head distance are largely consistent with User Study 1, with the largest distances observed in sitting and the shortest in lying. The difference from User Study 1 is that the variation of two dynamic

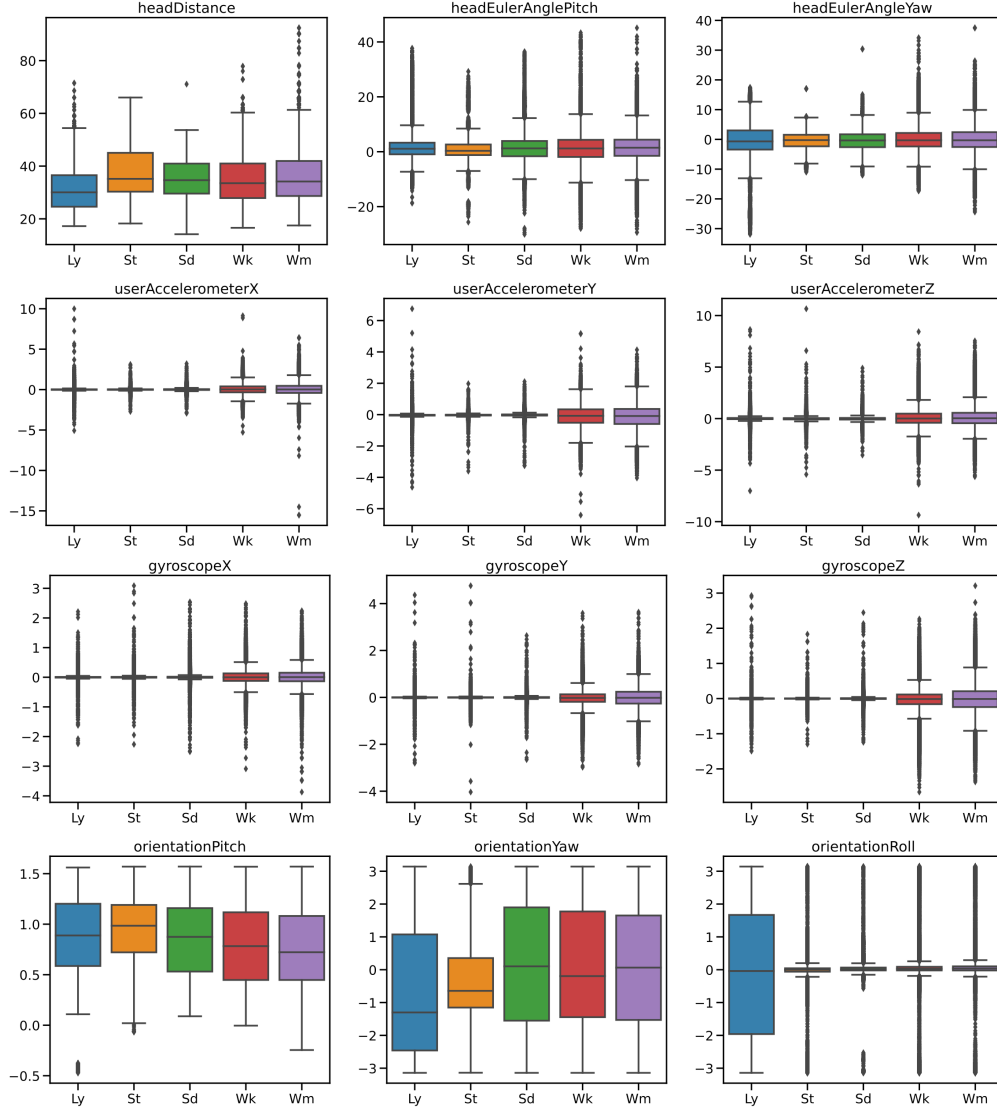


Figure 9: Box plots of motion data under each motion condition: *Ly* for lying, *St* for sitting, *Sd* for standing, *Wk* for walking and *Wm* for walking in maze.

conditions becomes larger, reaching a range similar to that of the sitting position; that is, sitting ($M = 37.62\text{cm}$, $SD = 9.47\text{cm}$), lying ($M = 31.03\text{cm}$, $SD = 7.43\text{cm}$), standing ($M = 35.22\text{cm}$, $SD = 7.13\text{cm}$), walking ($M = 34.51\text{cm}$, $SD = 8.77\text{cm}$), and walking in maze ($M = 35.52\text{cm}$, $SD = 9.72\text{cm}$). The difference in the mean values of two user studies is also small, changing from $M = 31.37\text{cm}$ to $M = 31.03\text{cm}$ in lying, $M = \pm 3.01\text{cm}$ in sitting, $M = \pm 4.15\text{cm}$ in standing, $M = \pm 3.44\text{cm}$ in walking, and $M = \pm 2.39\text{cm}$ in walking in maze.

Head Euler Angles (Pitch, Yaw): The pitch and yaw readings in User Study 2 align closely with those from User Study 1. Mean pitch angles across all conditions remained positive (range: 0.94° to 1.25°), with yaw angles close to 0° : lying ($M_{pitch} = 1.21$, $SD_{pitch} = 4.75$, $M_{yaw} = -0.86$, $SD_{yaw} = 6.84$), sitting ($M_{pitch} = 0.95$, $SD_{pitch} = 4.16$, $M_{yaw} = -0.44$, $SD_{yaw} = 2.89$), standing ($M_{pitch} = 1.24$, $SD_{pitch} = 5.34$, $M_{yaw} = -0.38$, $SD_{yaw} = 3.00$), walking ($M_{pitch} = 1.11$, $SD_{pitch} = 5.67$, $M_{yaw} = -0.01$, $SD_{yaw} = 3.93$), and walking in maze ($M_{pitch} = 1.25$, $SD_{pitch} = 0.01$, $M_{yaw} = 0.35$, $SD_{yaw} = 4.69$). But the variation of angle changes between motion conditions become smaller; for example, the range of SD_{pitch} is between 4.16 and 5.78, while that in user study 1 is between 7.68 and 10.72. The range of SD_{yaw} is between 2.89 and 6.84 while that in user study 1 is between 5.20 and 10.96. The difference in variation may be due to the difference in the weights (two phones in user study 1 vs. 1 phone in user study 2) and the length of the experiment; i.e. the duration of user study 2 was longer than user study 1, shown in Table 3 and Table 4. In addition, user study 2 requires a calibration process and testing, where participants try to keep their

device holding posture stable to execute the calibration and 9-point testing. This results in a smaller variation in the IMU readings.

User accelerometer and gyroscope: Mean accelerometer and gyroscope readings remained consistent with User Study 1, with values close to 0. Specifically, the changes of SD in user accelerometer and gyroscope, across the three axes and the all motion conditions of two user study experiments, are less than 0.45 and 0.34, respectively.

Orientation (Pitch, Yaw, Roll): User Study 2 exhibited larger means and variances in orientation compared to User Study 1, that is, lying ($M_{Pitch} = 0.87$, $SD_{Pitch} = 0.40$, $M_{Yaw} = -0.72$, $SD_{Yaw} = 1.93$, $M_{Roll} = -0.16$, $SD_{Roll} = 2.04$), sitting ($M_{Pitch} = 0.94$, $SD_{Pitch} = 0.33$, $M_{Yaw} = -0.39$, $SD_{Yaw} = 1.18$), $M_{Roll} = -0.18$, $SD_{Roll} = 0.87$), standing ($M_{Pitch} = 0.85$, $SD_{Pitch} = 0.37$, $M_{Yaw} = 0.13$, $SD_{Yaw} = 2.01$), $M_{Roll} = -0.01$, $SD_{Roll} = 0.45$), walking ($M_{Pitch} = 0.80$, $SD_{Pitch} = 0.39$, $M_{Yaw} = -0.05$, $SD_{Yaw} = 1.78$), $M_{Roll} = 0.09$, $SD_{Roll} = 0.78$), and walking in maze ($M_{Pitch} = 0.77$, $SD_{Pitch} = 0.08$, $M_{Yaw} = 0.03$, $SD_{Yaw} = 1.78$), $M_{Roll} = 0.08$, $SD_{Roll} = 0.66$). This may be attributed to participants more consciously altering their postures in response to cues, particularly evident in the continuous and stable body rolls observed during the lying condition.

To further examine the relationships between motion conditions in User Studies 1 and 2, we present t-SNE plots in Figure 10. The left Figure 10a is an comparison overview of motion data in two user studies. The right Figure 10b shows the comparison under each motion condition, where two walking conditions in user study 2 are combined and compared to user study 1. These visualisations demonstrate a high degree of similarity in motion features between the two studies, validating the consistency of our experimental design and data collection methods.

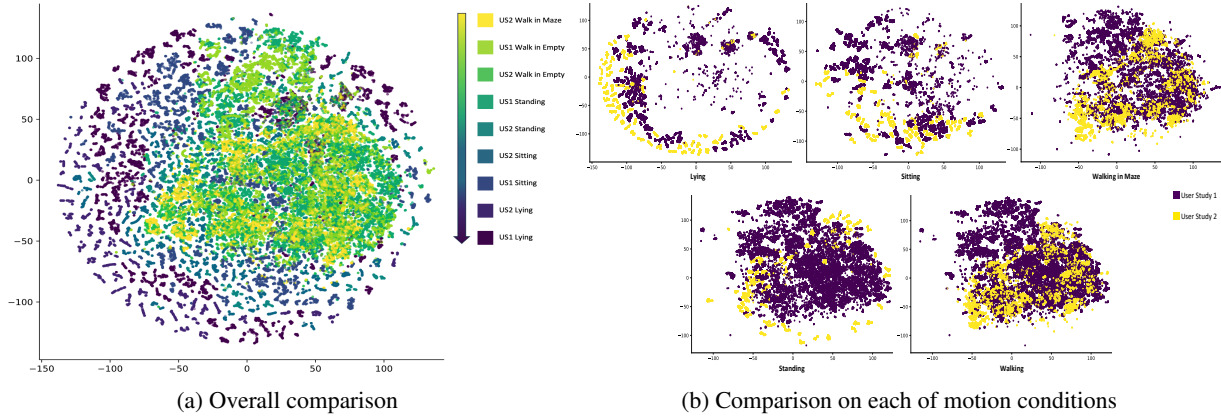


Figure 10: Cross-comparison t-SNE plots for User Study 1 and 2

6.2.2 Impact of Mobility on 2D Gaze Estimation

To assess the impact of mobility on 2D gaze estimation pipeline (base model performance and after calibrated performance) accuracy. We designed a series of personal-specific calibration approaches with varying granularities, from tasks to motion conditions. Figure 11 presents the overview of person-specific training and test procedure in collected data.

First we conduct an in-depth analysis by comparing the gaze estimation performance on two settings: (1) *base model performance*; that is, directly inputting the facial landmarks and facial images to the iTracker model in Section 3.1 and obtaining the gaze points; (2) *one-off calibration approach*; that is, training one calibrator using any of the calibration data following the procedure in Section 3.2 and then using this calibrator for gaze point prediction. This references the default procedure of commercial eye-trackers [51, 17], where a calibration is performed once before using the eye-tracker, and then the same calibrator is applied until the entire experiment is completed.

The 2D gaze estimation performance measured by calculating the Euclidean distance error in centimetres (cm), i.e. Root Mean Squared Error (RMSE), to quantify the discrepancy between the predicted gaze points and the ground truth: $RMSE = \sqrt{\frac{1}{n} \sum_{i=1}^n (gt_i - \hat{p}_i)^2}$, where gt_i and \hat{p}_i are the i th ground truth and estimated points and n is the total number of samples. Table 7 compares RMSE for base model and one-off calibrator, averaged on all the participants. For the one-off calibrator on each motion condition, we use each of 5 calibration data to train a calibrator and test on all the 5 test data, and then average the 5 test results.

Lying		Sitting		Standing		Walking		Walking in Maze	
Calibrator	9-Point Test	Calibrator	9-Point Test	Calibrator	9-Point Test	Calibrator	9-Point Test	Calibrator	9-Point Test
$C_{ly,1}$	$T_{ly,1}$	$C_{st,1}$	$T_{st,1}$	$C_{sd,1}$	$T_{sd,1}$	$C_{wk,1}$	$T_{wk,1}$	$C_{wm,1}$	$T_{wm,1}$
$C_{ly,2}$	$T_{ly,2}$	$C_{st,2}$	$T_{st,2}$	$C_{sd,2}$	$T_{sd,2}$	$C_{wk,2}$	$T_{wk,2}$	$C_{wm,2}$	$T_{wm,2}$
$C_{ly,3}$	$T_{ly,3}$	$C_{st,3}$	$T_{st,3}$	$C_{sd,3}$	$T_{sd,3}$	$C_{wk,3}$	$T_{wk,3}$	$C_{wm,3}$	$T_{wm,3}$
$C_{ly,4}$	$T_{ly,4}$	$C_{st,4}$	$T_{st,4}$	$C_{sd,4}$	$T_{sd,4}$	$C_{wk,4}$	$T_{wk,4}$	$C_{wm,4}$	$T_{wm,4}$
$C_{ly,5}$	$T_{ly,5}$	$C_{st,5}$	$T_{st,5}$	$C_{sd,5}$	$T_{sd,5}$	$C_{wk,5}$	$T_{wk,5}$	$C_{wm,5}$	$T_{wm,5}$

Calibrators	Train data	Test data (within)	Test data (between)
One-off calibration approach	One calibration data for each motion condition: $C_{m,i}$, where $m \in \{ly, st, sd, wk, wm\}$, $i \in [1,5]$	$T_m = \{T_{m,1}, T_{m,2}, T_{m,3}, T_{m,4}, T_{m,5}\}$, where $m \in \{ly, st, sd, wk, wm\}$	
Task-specific calibration approach	One calibration under m: $C_{m,i}$, where $m \in \{ly, st, sd, wk, wm\}$ and $i \in [1,5]$	Within-task: $T_{m,i}$	Between-task: $T_{m,j} \cup T_n, n \in \{ly, st, sd, wk, wm\}$ and $n \neq m, j \in [1,5]$ and $j \neq i$
Motion-specific calibration approach	30% of one test data under m: 30% of $T_{m,i}$, where $m \in \{ly, st, sd, wk, wm\}$ and $i \in [1,5]$	Within-motion: 70% of $T_{m,i}$	Between-motion: $T_{m,j} \cup T_n, n \in \{ly, st, sd, wk, wm\}$ and $n \neq m, j \in [1,5]$ and $j \neq i$

Figure 11: Person-specific training and test regime of calibrations in different granularities for each motion condition

We conducted a repeated-measures ANOVA to examine the effect of motion condition (*lying, sitting, standing, walking, walking in maze*) on the gaze estimation error. Mauchly’s test of sphericity was satisfied ($\chi^2(9) = 6.10, p = 0.19$). The ANOVA revealed a *significant main effect* of motion condition on error ($F(4, 36) = 7.42, p < .001, \eta_p^2 = .34$). Post-hoc pairwise comparisons using Holm-Bonferroni correction confirmed that errors under dynamic conditions (*walking, walking in maze*) were significantly higher than in static conditions (*lying, sitting*) (all $p < .05$). Additionally, to quantify practical significance, we computed Cohen’s d for each pairwise comparison, with values ranging from 0.60 to 0.95, indicating moderate to large effect sizes for the impact of motion on accuracy.

RMSE (cm) \ Scenario	Scenario					
	Average	Lying	Sitting	Standing	Walking	Walking in Maze
System						
Base Model	4.49 (2.76)	4.13 (2.45)	4.41 (2.93)	4.48 (2.77)	4.54 (2.64)	4.88 (2.88)
One-off Calibration	3.44 (2.19)	3.53 (2.18)	3.07 (1.97)	3.24 (2.05)	3.56 (2.29)	3.79 (2.44)

Table 7: Comparison of RMSE (mean and std in brackets) for base model and one-off calibration

Base model performance. The base model of our Eye Tracking Module serves as a benchmark for uncalibrated performance. It operates on the pre-train parameters from the third-party dataset and fine-tuned on experiment device specific data of RGBDGaze dataset [4]. The results in Table 7 show that the base model exhibits significant errors. The highest error is 4.88 cm on walking in a maze condition, and is a considerable deviation from the desired performance level. Therefore, it indicates that the base model, without additional calibration, is impractical for an eye-tracking system, particularly under dynamic conditions.

One-off calibration approach performance.

The one-off calibration approach offers some improvements, but the error remains sub-optimal. Similar to the base model, the one-off calibrator achieves the best performance on the sitting condition (i.e., 3.07 cm), and the worst performance on the walking in maze condition (i.e., 3.79 cm). The results also indicate higher transferability between postures under the sitting condition; that is, i.e., the range of head movements was similar in these conditions. However, this is not the case on the dynamic conditions.

Task-specific calibration approach performance. To address the limitations of the one-off calibration approach, we investigated a task-specific calibration approach. This method, illustrated in Figure 11, allows the model to learn task-relevant body and head behaviours, enabling us to further examine the impact of behavioural changes on model accuracy.

We designed experiments to evaluate model on both *within-task* and *between-task* scenarios’ performance. For each motion condition, we randomly selected one out of five calibration data to train a calibrator. We then tested this calibrator on its corresponding test data (reported as *within-task* errors) and on the other four test data (reported as *between-task* errors). This process was iterated for each calibration data, and the error resulting in cm were averaged. Figure 12 presents task-specific calibration approach performance on within-task and between-task scenarios.

Compared to the one-off calibration approach, task-specific calibration approach on within-task scenario reduce the errors from 3.07 cm to 2.57 cm on sitting, 3.53 cm to 2.96 cm on lying, 3.24 cm to 2.81 cm on standing, 3.56 cm to 3.10 cm on walking slowly, and 3.79 cm to 3.47 cm on walking in maze. On average, the improvement is 0.45 cm on

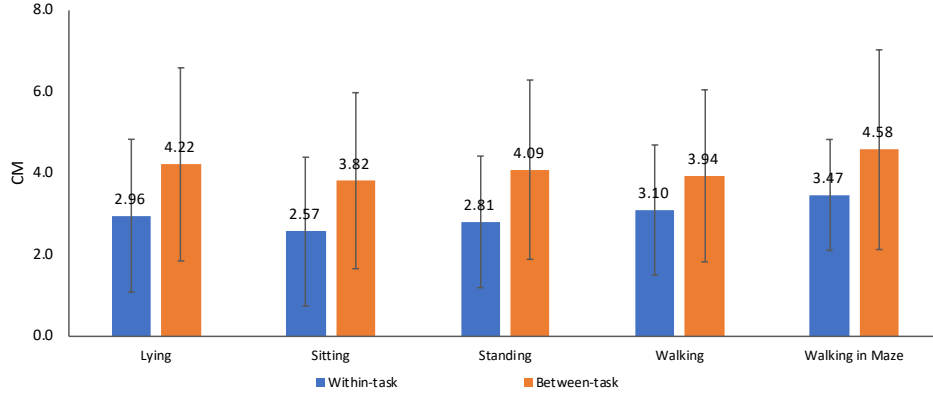


Figure 12: Comparison of RMSE for within-task and between-task scenarios

all the conditions; i.e., 13.41% from the one-off calibration approach performance. In the sitting condition, the error is close to the test error on GazeCapture dataset; i.e., 2.05 cm. However, most of the conditions have not yet achieved this accuracy, due to the natural difference in postures during calibration and testing. Figure 13 presents t-SNE plots of calibration and test data on each motion condition aggregated on all the participants. There is distribution shift in the motion data between calibration and testing stage indicate head and body behaviour differences between the two phases.

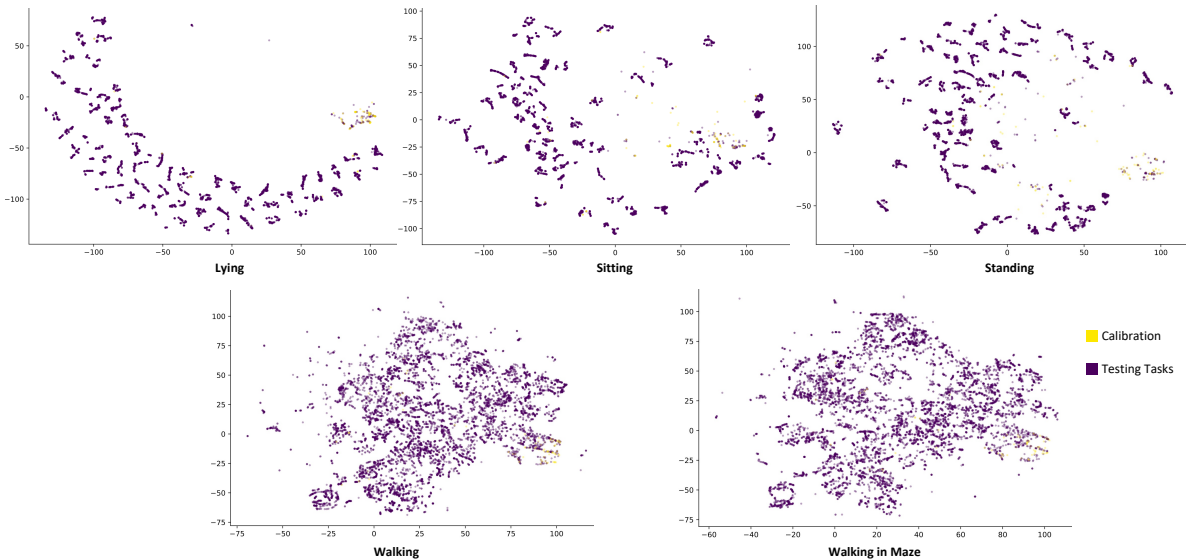


Figure 13: t-SNE plots of motion data of calibration and test dataset under each motion condition

Motion-specific calibration approach performance. To further reduce errors, we implemented a motion-specific calibration approach, which represents the finest-grained calibration method achievable in our study. This approach allows the model to learn a wider range of body and head behaviours within a single training session. For each motion condition, we utilised 30% of all the 9-point motion condition data to train a calibrator and tested it on the remaining 70% of the data from the same motion condition reported as *within-motion* errors. We also tested this calibrator on all other test sets of other motion conditions reported as *between-motion* errors. This process was iterated five times for each motion condition, and the performance results were averaged.

The motion-specific calibration approach achieved high accuracy, with errors of less than 2 cm in stable conditions, but under dynamic conditions the error increases to 2.73 cm, dropping by nearly 48.91%. This represents a 36.15% reduction in error compared to the one-off calibration approach. These results suggest an upper limit of performance in our study and they indicate that the model can greatly improve its performance by appreciating more body and head movements.

Table 8 illustrates how the motion-specific calibration approach performs across different motion conditions, highlighting the impact of motion variability on gaze estimation accuracy. The diagonal values show the lowest error rates (1.78

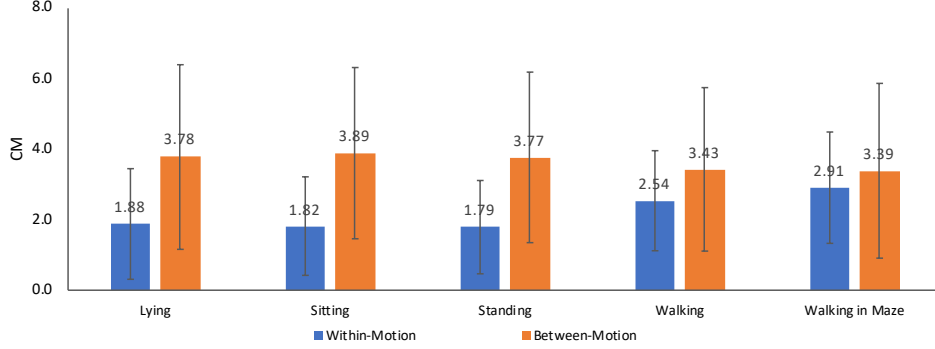


Figure 14: Comparison of RMSE for within-motion and between-motion conditions

cm to 2.91 cm) across all conditions, indicating that models perform best when tested on the same condition they were trained on. However, performance degrades when models are applied across different conditions, even between seemingly similar static conditions like sitting and standing (e.g., sitting model error increases from 1.82 cm to 3.36 cm when applied to standing). This degradation is more pronounced between static and dynamic conditions, and particularly notable for the lying condition. These results demonstrate that the generalisation of the model is strongly influenced by the extent and type of head and body movements captured in the training data, supporting the need for motion-specific approaches in mobile gaze estimation to account for motion pattern variability.

RMSE(cm) \ Train	Lying	Sitting	Standing	Walking	Walking in Maze
Test					
Lying	1.88 (1.57)	3.89 (2.27)	3.75 (2.11)	3.50 (2.10)	3.59 (2.06)
Sitting	3.52 (2.04)	1.82 (1.39)	3.36 (1.96)	3.29 (1.94)	3.31 (1.97)
Standing	3.49 (2.01)	3.31 (2.06)	1.78 (1.32)	3.19 (2.01)	3.21 (1.95)
Walking	3.89 (2.41)	4.05 (2.39)	3.86 (2.34)	2.54 (1.42)	3.46 (2.51)
Walking in maze	4.22 (2.33)	4.31 (2.44)	4.12 (2.43)	3.73 (2.33)	2.91 (1.58)

Table 8: Comparison of RMSE (mean and std in brackets) for between-motion-state experiments

6.2.3 Impact factor identification.

Our analysis has demonstrated that motion conditions and postures significantly impact mobile gaze estimation accuracy. To identify the key factors contributing to performance degradation, we employ a linear regression-based method. This approach allows us to quantify the relationship between various sensor features and gaze estimation error.

We curate a dataset using sensor features as input and the distance between predicted and ground truth gaze points as the target variable. Following the feature extraction procedure outlined in Section 5.6, we train calibrators using 30% of the test data from each motion condition. These calibrators are then used to predict gaze points on the remaining 70% of test data within the same condition and all test data from other conditions. Given the high dimensionality of our dataset (552 features across various sensors), we employ the Lasso (Least Absolute Shrinkage and Selection Operator) regression model. Lasso is particularly suited for this analysis as it handles multicollinearity and performs automatic feature selection by assigning zero coefficients to less important features. We use LassoCV from sklearn with cross-validation and optimal alpha parameter selection to enhance the robustness of our results.

Table 9 presents the top-ranked features identified by our regression analysis for both between-motion (a) and within-motion (b) conditions. The results reveal the following key points. (1) *Head Distance Dominance*: Across all motion conditions, head distance emerges as the most critical factor influencing gaze estimation accuracy. Its regression coefficient is consistently 4-5 times higher than the second-ranked feature. (2) *Motion-Specific Factors*: For the lying condition, additional important factors include synthetic mean of magnetometer (X, Y, Z), head Euler Angle, and synthetic mean of orientation (X, Y, Z). These factors reflect the unique mobility characteristics of the lying posture. (3) *Common Factors Across Conditions*: For sitting, standing, and walking conditions, common influential factors include magnetometer readings and cross-channel features of head Euler Angle (Y and Z) and orientation (X and Y). This suggests that the relative orientation and angles between the head and phone are more critical than absolute positional data. (4) *Consistency Across Analysis*: There is high consistency in the identified impact factors between the “within” and “between” motion condition analyses, demonstrating the robustness of our findings.

In addition, we aggregate the total Lasso coefficients to quantify the contribution of three major groups: *head distance*, *head movements* (sum of headEulerAngle features), and *device orientation deflection* (orientation + magnetometer features). For the *between-motion* model, the total Lasso-coefficient sum is 27.29, of which head distance contributes 9.79 ($\approx 35.87\%$), head movements 2.78 ($\approx 10.19\%$), and device orientation deflection 10.44 ($\approx 38.26\%$). Similarly, in the *within-motion* model (sum = 153.67), head distance is 46.39 ($\approx 30.19\%$), head movements 24.97 ($\approx 16.25\%$), and device orientation 49.78 ($\approx 32.39\%$). These three collectively account for more than 75% of the total Lasso weight in both conditions, underscoring head and device orientation as the primary drivers of 2D gaze-estimation errors.

(a) Between motion condition							(b) Within motion condition						
Sensor Feature	Avg	Ly	Si	St	Wa	Wm	Sensor Feature	Avg	Ly	Si	St	Wa	Wm
headDistance	9.79	18.09	4.86	9.98	11.43	4.59	headDistance	46.39	50.75	71.38	25.11	34.56	50.13
magnetometer	2.66	5.63	3.66	2.05	0.11	1.86	headEulerAngle	14.44	26.26	19.99	12.49	9.84	3.61
orientation	1.51	0.62	6.87	0.00	0.00	0.05	magnetometer	12.31	14.48	15.74	15.49	6.44	9.40
headEulerAngle	1.42	4.65	2.35	0.09	0.00	0.00	orientation	8.24	10.39	2.64	16.19	5.88	6.10
orientationXZ	0.93	2.44	0.53	1.51	0.03	0.16	headEulerAngleYZ	5.91	10.19	7.39	5.57	3.56	2.87
magnetometerXZ	0.91	2.27	0.67	0.98	0.20	0.45	orientationXZ	4.52	5.29	5.69	4.84	4.06	2.71
headEulerAngleYZ	0.89	1.83	0.87	0.98	0.26	0.52	magnetometerXZ	4.08	8.74	3.13	4.10	3.27	1.19
accelerometerYZ	0.89	1.32	1.92	0.96	0.23	0.00	magnetometerXY	3.78	5.73	3.56	3.64	3.38	2.63
accelerometerXZ	0.79	1.19	1.27	1.31	0.09	0.08	accelerometerXZ	3.21	5.40	5.80	2.23	2.03	0.59
orientationXY	0.53	1.01	0.56	1.07	0.00	0.00	orientationYZ	3.13	0.55	3.33	4.19	4.61	2.97
magnetometerYZ	0.50	0.72	1.01	0.43	0.18	0.17	accelerometerXY	3.06	3.30	6.78	2.04	1.82	1.36
accelerometerXY	0.48	0.22	0.34	1.33	0.11	0.43	magnetometerYZ	2.83	4.59	3.28	1.06	2.23	2.99
userAccelerometerXY	0.45	0.85	0.91	0.47	0.00	0.03	orientationXY	2.65	2.52	4.72	0.72	4.24	1.03
magnetometerXY	0.44	0.88	0.48	0.54	0.03	0.26	headEulerAngleZ	2.39	3.75	3.09	2.21	2.02	0.90
gyroscopeYZ	0.38	1.20	0.41	0.12	0.11	0.05	headEulerAngleY	2.23	2.64	2.82	2.92	1.78	0.98
orientationYZ	0.35	0.82	0.36	0.26	0.24	0.08	magnetometerX	2.23	2.57	5.16	1.34	1.41	0.65
magnetometerZ	0.34	0.60	0.62	0.42	0.00	0.06	gyroscopeXY	2.21	2.33	2.89	1.26	1.18	3.39
magnetometerX	0.34	0.66	0.48	0.36	0.01	0.19	gyroscopeYZ	2.16	2.59	2.72	0.57	2.28	2.65
headEulerAngleY	0.29	0.68	0.43	0.24	0.03	0.10	accelerometerYZ	2.00	0.79	2.23	0.20	3.67	3.11
orientationYaw	0.29	0.35	0.51	0.40	0.03	0.15	accelerometerX	1.98	3.17	3.43	1.80	0.78	0.70
accelerometerY	0.24	0.40	0.54	0.22	0.02	0.05	gyroscopeXZ	1.90	2.35	3.29	0.75	1.65	1.44
accelerometerZ	0.24	0.57	0.35	0.26	0.01	0.02	accelerometer	1.87	4.59	0.09	0.51	4.15	0.00
gyroscopeXZ	0.24	0.43	0.23	0.42	0.00	0.11	userAccelerometerYZ	1.72	3.77	2.69	0.39	0.77	0.98
gyroscopeXY	0.23	0.55	0.18	0.42	0.00	0.00	magnetometerZ	1.70	2.22	3.85	0.84	1.09	0.50
magnetometerY	0.23	0.31	0.43	0.25	0.00	0.13	userAccelerometerXY	1.66	2.39	2.76	0.59	1.46	1.09
accelerometerX	0.22	0.28	0.41	0.34	0.03	0.03	accelerometerZ	1.62	3.22	1.02	0.61	2.24	1.00
userAccelerometerYZ	0.21	0.60	0.35	0.02	0.00	0.09	userAccelerometerXZ	1.45	2.15	2.47	0.21	1.00	1.42
headEulerAngleZ	0.17	0.41	0.28	0.11	0.01	0.05	accelerometerY	1.32	1.15	1.10	1.06	2.17	1.09
userAccelerometerY	0.15	0.29	0.23	0.17	0.01	0.05	gyroscope	1.31	0.00	0.07	0.29	6.20	0.00
userAccelerometerZ	0.13	0.22	0.22	0.21	0.00	0.01	orientationYaw	1.11	2.40	1.08	0.94	0.76	0.36
aggVelocity	0.13	0.25	0.18	0.20	0.01	0.01	magnetometerY	1.10	1.63	1.65	0.88	0.79	0.53
gyroscope	0.13	0.00	0.28	0.30	0.00	0.06	orientationRoll	1.09	1.32	1.45	1.14	0.76	0.77
aggHoldAngle	0.12	0.27	0.06	0.27	0.00	0.00	orientationPitch	1.01	0.96	2.00	0.26	1.18	0.65
orientationRoll	0.11	0.21	0.17	0.13	0.01	0.04	userAccelerometerZ	0.70	0.76	1.21	0.23	0.87	0.42
gyroscopeY	0.10	0.27	0.14	0.07	0.00	0.05	aggHoldAngle	0.69	0.82	0.89	0.24	1.30	0.22
gyroscopeX	0.10	0.24	0.19	0.06	0.00	0.03	gyroscopeY	0.69	0.66	1.28	0.20	0.91	0.42
userAccelerometerXZ	0.10	0.30	0.07	0.08	0.00	0.06	userAccelerometerX	0.68	0.82	1.18	0.35	0.71	0.33
userAccelerometerX	0.10	0.13	0.19	0.14	0.00	0.03	userAccelerometerY	0.65	0.84	1.13	0.27	0.58	0.41
gyroscopeZ	0.06	0.15	0.06	0.05	0.00	0.04	gyroscopeX	0.58	0.81	0.75	0.56	0.57	0.23
orientationPitch	0.05	0.04	0.14	0.06	0.00	0.02	gyroscopeZ	0.55	0.52	0.73	0.24	0.99	0.29
userAccelerometer	0.02	0.03	0.04	0.02	0.00	0.00	aggVelocity	0.51	0.50	0.65	0.33	0.77	0.32
accelerometer	0.00	0.00	0.02	0.00	0.00	0.00	userAccelerometer	0.01	0.00	0.00	0.01	0.03	0.00

Table 9: Impact factors identified *between* and *within* motion conditions

7 Discussion

Our studies offer an empirical analysis of user-device interaction under varying motion states, shedding light on the core limitations of 2D gaze estimation in mobile contexts, particularly regarding head-movement adaptation. By examining both low-level sensor signals (e.g. accelerometer, gyroscope) and higher-level behavioural patterns (in-task vs. switch-task, within- vs. between-motion conditions), we highlight the need for more robust and adaptive eye-tracking systems on handheld devices. Below, we discuss the main takeaways and potential paths forward.

7.1 Behaviour Patterns in Mobile Interaction

7.1.1 Sensor data analysis and insights

The analysis of sensor data, including head distance, Euler angles, accelerometer, gyroscope, and magnetometer readings, reveals the complex nature of mobile interactions. The consistency in head distance across different mobility

states suggests that users subconsciously attempt to stabilise their view. However, the variability in gyroscope and accelerometer data reflects the frequent adjustments made during motion.

7.1.2 Clustering distribution and user behaviour

Through t-SNE visualisations and clustering, we observe distinct behavioural patterns between static (e.g. lying, sitting) and dynamic (e.g. walking) activities. This aligns with the findings of Sugano et al. [49] on desktop systems, but our work extends this concept to the more challenging domain of mobile devices.

7.1.3 In-Task vs. Switch-Task dynamics

A key insight is the contrast between *in-task* stability and *switch-task* variability. During continuous engagement with a single activity (e.g. reading, scrolling), head pose remains moderately consistent. However, once a task ends or changes, rapid reorientation spikes the error. Head distance can fluctuate by up to 10 cm, and device angles shift abruptly.

7.2 Limitations of 2D gaze estimation in handling dynamic head poses

Our study provides empirical evidence that 2D gaze estimation methods, while popular for their simplicity, are particularly vulnerable to changes in head pose. This weakness stems from the fundamental assumption in 2D approaches that the model can implicitly learn to handle head pose variations without explicit normalisation or modelling.

- *Between-motion scenario*: When users transition across different motion states (e.g. from sitting to walking), head movements, device orientation changes, and increased screen distance collectively account for over 70% of the variance in gaze error.
- *Within-motion scenario*: Even within a single motion state, micro-movements, such as the trembling while typing and the swaying of the wrist, explain significant error. Our Lasso regression shows that head distance, head movements, and orientation deflection comprise about 80% of the regression-weight sum, implying that small head or device tilt changes still degrade accuracy.

This vulnerability arises largely because most 2D methods lack explicit head pose modelling (e.g. no normalisation akin to 3D geometry). Therefore, they cannot seamlessly adapt when the user’s face or device orientation drifts beyond the training sample distribution.

7.2.1 Implications for mobile eye tracking

A one-off calibration is often insufficient for highly dynamic daily usage. Our data suggests that small posture shifts or task switches can degrade errors by up to 2 or 3 times. A more adaptive calibration approach to periodically re-estimates the user’s head pose or normalises on-screen coordinates is crucial for robust performance. Incorporating orientation and head-distance data directly into the 2D pipeline may help enhance the resilience. This practice of handle head pose explicitly is often used in 3D gaze estimation pipeline. Frequent manual calibrations can disrupt flow, leading to *calibration fatigue*. The approach therefore needs to be combined with natural human-device interaction to explore *implicit calibration cues*; e.g., using known UI elements where the user must look to avoid user burden issues.

7.3 Limitations

Our study has several limitations that provide opportunities for future research.

Sample size. Our current participant pool (10 in total) offers preliminary insights but may not capture the full variance in anthropometrics, cultural usage patterns, or visual impairments. Scaling up to more diverse user groups will increase generalizability and validate whether our findings hold for broader populations.

Experimental setup. While we attempted to simulate real-world conditions; e.g., lying, walking in a maze, these remain semi-controlled lab scenarios. Follow-up in-the-wild deployments or longer-term longitudinal studies would better capture unpredictable daily activities, lighting changes, and unstructured user behaviours.

Hardware integration. In User Study 1, we attached our experimental device to participants’ personal phones. Although this approach preserved their familiar interface and protected their privacy, the extra weight could affect posture and stability. Future designs might consider more integrated, lightweight hardware solutions.

Motion conditions. The slight discrepancy in motion conditions between User Studies 1 and 2 (four vs. five conditions) may affect cross-study comparison. Standardising conditions across studies would be beneficial in future research to provide a more consistent evaluation of 2D gaze estimation limitations.

Gaze estimation approach comparison. Our use of a classic 2D gaze estimation pipeline [33, 8] without data normalisation or explicit head pose handling like 3D methods, exemplifies the limitations of current 2D approaches. Future work should compare the generalization ability of 2D and 3D gaze estimation techniques on a more directly way; i.e., complementing 2D and 3D labels under one dataset and test 2D to 3D, 3D to 2D, as well as test their domain adaptation capabilities on different datasets; i.e. different source and target domains.

7.4 Future Direction of 2D Gaze Estimation

Continuous calibration for 2D gaze estimation based eye tracking system A single calibration does not allow the 2D gaze estimation model to obtain enough user-device interaction data for generalization performance that supports high-precision prediction in different scenarios of device usage. To obtain sufficient data for generalization, the 2D gaze estimation methods need to take multiple calibrations to incrementally and continuously update the model.

Some projects are starting to look into this direction; for example, Sugano et al. [49] employ incremental learning for gaze estimation in a desktop environment, which learns and clusters interaction patterns with the desktop to improve performance. However, most existing solutions target desktop or static contexts. Future work must adapt these ideas to address higher variability in mobile device usage; e.g., combining inertial sensor triggers with automatic detection of posture shifts to prompt subtle re-calibration.

Toward a 2D-3D hybrid approach Finally, bridging 2D and 3D paradigms may yield a powerful hybrid method that retains 2D’s simplicity while leveraging partial geometric cues. For instance, an algorithm could estimate head orientation in a lightweight fashion, then project or normalise the face region for stable 2D inference, thereby mitigating large off-axis head poses without a full 3D camera normalization. Such a pipeline could drastically cut computational cost relative to full 3D solutions yet still handle bigger pose shifts than conventional 2D methods.

Overall, our results concludes that explicitly modelling head and device orientation remains the largest unmet need in 2D gaze estimation for mobile devices. By incorporating adaptive calibration, domain transfer, and partial 3D normalisation techniques, 2D methods can move closer to the accuracy and robustness required for real-world mobile eye-tracking applications.

8 Conclusion

This study provides empirical evidence on the limitations of 2D gaze estimation methods in mobile contexts, particularly their vulnerability to head pose and device orientation variations. By combining motion (IMU) and vision data, we demonstrate that 2D gaze estimators struggle to handle the frequent orientation changes characteristic of real-world mobile device usage. Through two comprehensive user studies investigating the spatial dynamics of user-device interactions, we show that the assumption that models can implicitly learn to compensate for head pose variations proves inadequate in dynamic mobile scenarios. These findings highlight the need for more advanced, adaptive eye-tracking systems that can explicitly account for head movements and maintain accuracy across diverse usage contexts. Future research should focus on developing novel approaches that address these limitations, potentially by incorporating elements of 3D gaze estimation or explicit head pose modelling into more efficient 2D frameworks that explore 2D-3D hybrid pipelines that balance real-time performance with energy efficiency.

References

- [1] ADAMCZYK, P. D., AND BAILEY, B. P. If not now, when? the effects of interruption at different moments within task execution. In *Proceedings of the SIGCHI conference on Human factors in computing systems* (2004), pp. 271–278.
- [2] ALEXIEV, K., TOSHKOV, T., AND DOJNOW, P. Enhancing accuracy and precision of eye tracker by head movement compensation and calibration. In *Proceedings of the 20th International Conference on Computer Systems and Technologies* (2019), pp. 226–233.
- [3] ANGUITA, D., GHIO, A., ONETO, L., PARRA, X., REYES-ORTIZ, J. L., ET AL. A public domain dataset for human activity recognition using smartphones. In *Esann* (2013), vol. 3, p. 3.
- [4] ARAKAWA, R., GOEL, M., HARRISON, C., AND AHUJA, K. Rgbgaze: Gaze tracking on smartphones with rgb and depth data. In *Proceedings of the 2022 International Conference on Multimodal Interaction* (2022), pp. 329–336.

- [5] BÂCE, M., STAAL, S., AND BULLING, A. Accurate and robust eye contact detection during everyday mobile device interactions. *arXiv preprint arXiv:1907.11115* (2019).
- [6] BÂCE, M., STAAL, S., AND BULLING, A. Quantification of users' visual attention during everyday mobile device interactions. In *Proceedings of the 2020 CHI Conference on Human Factors in Computing Systems* (2020), pp. 1–14.
- [7] BALIM, H., PARK, S., WANG, X., ZHANG, X., AND HILLIGES, O. Efe: End-to-end frame-to-gaze estimation. In *Proceedings of the IEEE/CVF Conference on Computer Vision and Pattern Recognition* (2023), pp. 2687–2696.
- [8] BAO, Y., CHENG, Y., LIU, Y., AND LU, F. Adaptive feature fusion network for gaze tracking in mobile tablets. In *2020 25th International Conference on Pattern Recognition (ICPR)* (2021), IEEE, pp. 9936–9943.
- [9] BLIGNAUT, P. Idiosyncratic feature-based gaze mapping. *Journal of Eye Movement Research* 9, 3 (2016).
- [10] CHENG, Y., AND LU, F. Gaze estimation using transformer. In *2022 26th International Conference on Pattern Recognition (ICPR)* (2022), IEEE, pp. 3341–3347.
- [11] CHENG, Y., WANG, H., BAO, Y., AND LU, F. Appearance-based gaze estimation with deep learning: A review and benchmark. *IEEE Transactions on Pattern Analysis and Machine Intelligence* (2024).
- [12] CLAY, V., KÖNIG, P., AND KOENIG, S. Eye tracking in virtual reality. *Journal of eye movement research* 12, 1 (2019).
- [13] DREWES, H., PFEUFFER, K., AND ALT, F. Time- and space-efficient eye tracker calibration. In *Proceedings of the 11th ACM Symposium on Eye Tracking Research & Applications* (New York, NY, USA, 2019), ETRA '19, Association for Computing Machinery.
- [14] DUCHOWSKI, A. T., AND DUCHOWSKI, A. T. *Eye tracking methodology: Theory and practice*. Springer, 2017.
- [15] FOGARTY, J., HUDSON, S. E., ATKESON, C. G., AVRAHAMI, D., FORLIZZI, J., KIESLER, S., LEE, J. C., AND YANG, J. Predicting human interruptibility with sensors. *ACM Transactions on Computer-Human Interaction (TOCHI)* 12, 1 (2005), 119–146.
- [16] FUNES MORA, K. A., MONAY, F., AND ODOBEZ, J.-M. Eyediap: A database for the development and evaluation of gaze estimation algorithms from rgb and rgb-d cameras. In *Proceedings of the symposium on eye tracking research and applications* (2014), pp. 255–258.
- [17] GAZEPOINT. Tutorials for our eye-tracking technology, April 6 2022.
- [18] GHOSH, S., DHALL, A., HAYAT, M., KNIBBE, J., AND JI, Q. Automatic gaze analysis: A survey of deep learning based approaches. *IEEE Transactions on Pattern Analysis and Machine Intelligence* 46, 1 (2023), 61–84.
- [19] GOOGLE LLC. MI kit, March 2023.
- [20] GOOGLE LLC. Flutter - build apps for any screen. <https://flutter.dev>, 2024. Accessed: 2023 Jan 07.
- [21] HANSEN, D. W., AND JI, Q. In the eye of the beholder: A survey of models for eyes and gaze. *IEEE transactions on pattern analysis and machine intelligence* 32, 3 (2009), 478–500.
- [22] HUANG, H., REN, L., YANG, Z., ZHAN, Y., ZHANG, Q., AND LV, J. Gazeattentionnet: Gaze estimation with attentions. In *ICASSP 2022-2022 IEEE International Conference on Acoustics, Speech and Signal Processing (ICASSP)* (2022), IEEE, pp. 2435–2439.
- [23] HUANG, M. X., AND BULLING, A. Saccalib: Reducing calibration distortion for stationary eye trackers using saccadic eye movements. In *Proceedings of the 11th ACM Symposium on Eye Tracking Research & Applications* (New York, NY, USA, 2019), ETRA '19, Association for Computing Machinery.
- [24] HUANG, M. X., LI, J., NGAI, G., AND LEONG, H. V. Screenglint: Practical, in-situ gaze estimation on smartphones. In *CHI '17* (2017), ACM, p. 2546–2557.
- [25] HUANG, Q., VEERARAGHAVAN, A., AND SABHARWAL, A. Tabletgaze: dataset and analysis for unconstrained appearance-based gaze estimation in mobile tablets. *Machine Vision and Applications* 28, 5 (2017), 445–461.
- [26] HUYNH, S., BALAN, R. K., AND KO, J. imon: Appearance-based gaze tracking system on mobile devices. *IMWUT* 5, 4 (2021), 1–26.
- [27] JIANG, Z., HAN, J., QIAN, C., XI, W., ZHAO, K., DING, H., TANG, S., ZHAO, J., AND YANG, P. Vads: Visual attention detection with a smartphone. In *IEEE INFOCOM 2016-The 35th Annual IEEE International Conference on Computer Communications* (2016), IEEE, pp. 1–9.
- [28] KAUR, H., JINDAL, S., AND MANDUCHI, R. Rethinking model-based gaze estimation. *Proceedings of the ACM on computer graphics and interactive techniques* 5, 2 (2022), 1–17.

- [29] KELLNHOFER, P., RECASENS, A., STENT, S., MATUSIK, W., AND TORRALBA, A. Gaze360: Physically unconstrained gaze estimation in the wild. In *the IEEE/CVF International Conference on Computer Vision (2019)*, IEEE, pp. 6912–6921.
- [30] KHAMIS, M., ALT, F., AND BULLING, A. The past, present, and future of gaze-enabled handheld mobile devices: Survey and lessons learned. In *Proceedings of the 20th International Conference on Human-Computer Interaction with Mobile Devices and Services (2018)*, pp. 1–17.
- [31] KHAMIS, M., BAIER, A., HENZE, N., ALT, F., AND BULLING, A. Understanding face and eye visibility in front-facing cameras of smartphones used in the wild. In *CHI '18 (2018)*, ACM, p. 1–12.
- [32] KONG, A., AHUJA, K., GOEL, M., AND HARRISON, C. Eyemu interactions: Gaze+ imu gestures on mobile devices. In *Proceedings of the 2021 International Conference on Multimodal Interaction (2021)*, pp. 577–585.
- [33] KRAFKA, K., KHOSLA, A., KELLNHOFER, P., KANNAN, H., BHANDARKAR, S., MATUSIK, W., AND TORRALBA, A. Eye tracking for everyone. In *Proceedings of the IEEE conference on computer vision and pattern recognition (2016)*, pp. 2176–2184.
- [34] LEI, Y., HE, S., KHAMIS, M., AND YE, J. An end-to-end review of gaze estimation and its interactive applications on handheld mobile devices. *ACM Comput. Surv.* 56, 2 (sep 2023).
- [35] LEI, Y., WANG, Y., CASLIN, T., WISOWATY, A., ZHU, X., KHAMIS, M., AND YE, J. Dynamicread: Exploring robust gaze interaction methods for reading on handheld mobile devices under dynamic conditions. *Proceedings of the ACM on Human-Computer Interaction* 7, ETRA23 (5 2023), 17.
- [36] LEPOT, M., AUBIN, J.-B., AND CLEMENS, F. H. Interpolation in time series: An introductory overview of existing methods, their performance criteria and uncertainty assessment. *Water* 9, 10 (2017), 796.
- [37] LI, B., SNIDER, J. C., WANG, Q., MEHTA, S., FOSTER, C., BARNEY, E., SHAPIRO, L., VENTOLA, P., AND SHIC, F. Calibration error prediction: Ensuring high-quality mobile eye-tracking. In *2022 Symposium on Eye Tracking Research and Applications (2022)*, pp. 1–7.
- [38] LIU, J., CHI, J., HU, W., AND WANG, Z. 3d model-based gaze tracking via iris features with a single camera and a single light source. *IEEE Transactions on Human-Machine Systems* 51, 2 (2020), 75–86.
- [39] MARTSCHINKE, J., MARTSCHINKE, J., STAMMINGER, M., AND BAUER, F. Gaze-dependent distortion correction for thick lenses in hmds. In *2019 IEEE Conference on Virtual Reality and 3D User Interfaces (VR) (2019)*, IEEE, pp. 1848–1851.
- [40] MENGES, R., KUMAR, C., AND STAAB, S. Improving user experience of eye tracking-based interaction: Introspecting and adapting interfaces. *ACM Transactions on Computer-Human Interaction (TOCHI)* 26, 6 (2019), 1–46.
- [41] PALMERO, C., SELVA, J., BAGHERI, M. A., AND ESCALERA, S. Recurrent cnn for 3d gaze estimation using appearance and shape cues. In *29th British Machine Vision Conference, BMVC 2018 (2019)*.
- [42] PALMERO, C., SHARMA, A., BEHRENDT, K., KRISHNAKUMAR, K., KOMOGORTSEV, O. V., AND TALATHI, S. S. Openeds2020 challenge on gaze tracking for vr: Dataset and results. *Sensors* 21, 14 (2021), 4769.
- [43] PARK, S., MELLO, S. D., MOLCHANOV, P., IQBAL, U., HILLIGES, O., AND KAUTZ, J. Few-shot adaptive gaze estimation. In *Proceedings of the IEEE/CVF international conference on computer vision (2019)*, pp. 9368–9377.
- [44] PASZKE, A., GROSS, S., MASSA, F., LERER, A., BRADBURY, J., CHANAN, G., KILLEEN, T., LIN, Z., GIMELSHEIN, N., ANTIGA, L., ET AL. Pytorch: An imperative style, high-performance deep learning library. *Advances in neural information processing systems* 32 (2019).
- [45] PEDREGOSA, F., VAROQUAUX, G., GRAMFORT, A., MICHEL, V., THIRION, B., GRISEL, O., BLONDEL, M., PRETTENHOFER, P., WEISS, R., DUBOURG, V., ET AL. Scikit-learn: Machine learning in python. *the Journal of machine Learning research* 12 (2011), 2825–2830.
- [46] PI, J., AND SHI, B. E. Task-embedded online eye-tracker calibration for improving robustness to head motion. In *Proceedings of the 11th ACM Symposium on Eye Tracking Research & Applications (2019)*, pp. 1–9.
- [47] STEIL, J., MÜLLER, P., SUGANO, Y., AND BULLING, A. Forecasting user attention during everyday mobile interactions using device-integrated and wearable sensors. In *Proceedings of the 20th international conference on human-computer interaction with mobile devices and services (2018)*, pp. 1–13.
- [48] SUGANO, Y., MATSUSHITA, Y., AND SATO, Y. Learning-by-synthesis for appearance-based 3d gaze estimation. In *Proceedings of the IEEE conference on computer vision and pattern recognition (2014)*, pp. 1821–1828.
- [49] SUGANO, Y., MATSUSHITA, Y., SATO, Y., AND KOIKE, H. An incremental learning method for unconstrained gaze estimation. In *Computer Vision – ECCV 2008 (Berlin, Heidelberg, 2008)*, D. Forsyth, P. Torr, and A. Zisserman, Eds., Springer Berlin Heidelberg, pp. 656–667.

- [50] TEAM, B. Revealing average screen time statistics, March 11 2024.
- [51] TOBII. Get started with your eye tracker, April 24 2023.
- [52] TOBII LTD. How to calibrate and validate in tobii pro lab, September 5 2022.
- [53] VALLIAPPAN, N., DAI, N., STEINBERG, E., HE, J., ROGERS, K., RAMACHANDRAN, V., XU, P., SHO-JAEIZADEH, M., GUO, L., KOHLHOFF, K., ET AL. Accelerating eye movement research via accurate and affordable smartphone eye tracking. *Nature communications* 11, 1 (2020), 4553.
- [54] WOOD, E., AND BULLING, A. EYETAB: Model-based gaze estimation on unmodified tablet computers. In *Proceedings of the symposium on eye tracking research and applications* (2014), pp. 207–210.
- [55] ZHANG, X., PARK, S., BEELER, T., BRADLEY, D., TANG, S., AND HILLIGES, O. Eth-xgaze: A large scale dataset for gaze estimation under extreme head pose and gaze variation. In *Computer Vision—ECCV 2020: 16th European Conference, Glasgow, UK, August 23–28, 2020, Proceedings, Part V 16* (2020), Springer, pp. 365–381.
- [56] ZHANG, X., SUGANO, Y., AND BULLING, A. Revisiting data normalization for appearance-based gaze estimation. In *Proceedings of the 2018 ACM Symposium on Eye Tracking Research & Applications* (New York, NY, USA, 2018), ETRA '18, Association for Computing Machinery.
- [57] ZHANG, X., SUGANO, Y., AND BULLING, A. Revisiting data normalization for appearance-based gaze estimation. In *Proceedings of the 2018 ACM symposium on eye tracking research & applications* (2018), pp. 1–9.
- [58] ZHANG, X., SUGANO, Y., FRITZ, M., AND BULLING, A. Appearance-based gaze estimation in the wild. In *CVPR '15* (June 2015), IEEE, pp. 4511–4520.
- [59] ZHANG, X., SUGANO, Y., FRITZ, M., AND BULLING, A. It's written all over your face: Full-face appearance-based gaze estimation. In *Proceedings of the IEEE conference on computer vision and pattern recognition workshops* (2017), pp. 51–60.
- [60] ZHANG, X., SUGANO, Y., FRITZ, M., AND BULLING, A. Mpiigaze: Real-world dataset and deep appearance-based gaze estimation. *IEEE transactions on pattern analysis and machine intelligence* 41, 1 (2017), 162–175.
- [61] ZHANG, X., SUGANO, Y., FRITZ, M., AND BULLING, A. Mpiigaze: Real-world dataset and deep appearance-based gaze estimation. *IEEE Transactions on Pattern Analysis and Machine Intelligence* 41, 1 (2019), 162–175.